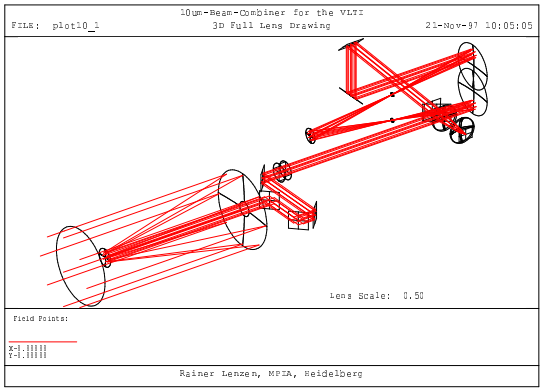

The mid-infrared interferometric instrument for the VLTI (MIDI)

Study group report for the steering committee meeting on December 9, 1997, prepared by

Christoph Leinert (Project scientist), Uwe Graser (Project manager)
Tom Herbst, Stefan Hippler
Reinhard Mundt, Rainer Lenzen, Eckhart Pitz
Irene Porro, Massimo Robberto
Ralf-Rainer Rohloff, Norbert Salm
Heidelberg

Vincent Coudé du Foresto, Guy Perrin, Meudon
Rudolf Le Poole, Huub Rottgering, Leiden
Bruno Lopez, Nice
Bringfried Stecklum, Jena
Oskar von der Lühe, Freiburg
Rens Waters, Amsterdam

December 11, 1997

Contents

Chapter 1

Introduction

This report on the mid-infrared interferometric instrument for the VLTI ("MIDI") follows the request that the steering committeee be provided, for its planned meeting of December 9, 1997, with more detailed optical designs and cost estimates for the four interferometric instruments currently under discussion.

This is the second report prepared by the working group for the "MIDI" instrument. It updates the information given in the previous report for the ISAC meeting on July 15, 1997. It concentrates on the technical aspects of the instrument and does not repeat the proposed scientific programmes discussed in July.

This document does not represent a formal milestone for the development of the mid-infrared interferometric instrument. Rather it describes the present status of the ongoing work towards a preliminary design for this instrument.

The study group will be transformed into an instrument team in due time. As shown in the author list, the Max-Planck-Institut für Astronomie has identified the persons who mainly are responsible for carrying through this beginning project.

Chapter 2

Extended summary

Additional information on the instrument can be found in the study group report to ISAC from July 13, 1997.

2.1 Priorities

The priorities have not changed since July:

- The main emphasis is on developing an instrument working in the 10 μm window with one baseline, measuring visibilities. The measuring modes include one aiming at good sensitivity, sacrificing accuracy; one aiming at good accuracy at the expense of reduced sensistivity; and at least one intermediate arrangement.

- A natural enhancement of the capabilities of the instrument would be the extension to the 20 μm range and to higher spectral resolution. The Dutch members of the study group are actively seeking the funds necessary to implement these options early in the project.

- For a second phase of the instrument development we consider it necessary to provide phase measurements: either by phase closure measurements with at least three input telescope beams or by tying the 10 μm instrument to the external phase-referencing instrument, or by both methods. At this stage also the simultaneous use of four telescopes will be considered.
  External fringe tracking is highly desired. For all sources with suitable spectrum and geometry it should provide substantial gains in sensitivity. We will try to have this possibility available already during the first phase of instrument operation.

2.2 Optical design

In general , the optical design for the mid-infrared interferometric instrument has to provide the following functions:

- to accept beams of 80 mm diameter,

- an image plane on the detector,
- the beam combination not too far from the pupil plane,
- very good suppression of thermal emission from the surroundings in laboratory, delay lines and telescopes,
- an image sharpness which puts most of the light on one pixel (to reduce readout noise),
- the possibility to introduce monomode fibers for beam cleaning,
- the possibility to extract photometric signals before beam combination,
- light inputs for verifying the interferometric operation of the instrument at 10 μm,
- acceptable complexity and preferably compact design,
- to allow - in principle - the inclusion of a third and forth beam for phase closure measurements.

The studies performed so far have shown that satisfying solutions can be found both with reflective and and with transmissive optics, which is an important result. The present design (chapter 4) in addition keeps the option to use most of the optical train both for 10 μm and for 20 μm observations, and it therefore mostly uses reflective optics. We still are discussing how much we gain on one side and how much we lose on the other side by making simultaneous 10 μm and 20 μm observations possible. In any case, a dedicated, sensitive 10 μm channel will be available in the instrument.

For phase closure measurements with three or four beams, the optics used for beam conbination and imaging onto the detector will have to undergo profound changes.

2.3 Detector

Array detectors of the needed dimensions of a few hundred pixels are available. Somewhat surprisingly, readout noise is not necessarily negligible even in the high background environment of the VLTI in the thermal infrared. This results from the limited well capacity of $\approx 10^7$ electrons for the available detector chips. We plan to buy the "science grade" detector late in the project in order to profit from expected improvements in well capacity and readout noise. Before, we intend to use "engineering type" detectors of lower quality for the development of the instrument.

2.4 Technical realisation

We want to profit as much as possible from several projects running at the Max-Planck-Institut für Astronomie:

- MAX – a 10 μm camera for UKIRT

– CONICA – the near-infrared high spatial resolution camera for the VLT

– OMEGA – two 1kx1k near-infrared array cameras with flexible readout electronics

In particular, the cryogenics concept and the instrument control system proposed in large part are adaptations of the solutions found for CONICA. The readout electronics developed for the OMEGA projects is flexible enough to be used also for the "MIDI" instrument, and the experience with the MAX array on the behaviour and characteristics of measured 10 μm signals is the basis on which the different measuring modes are being built.

The concept for data transfer, computing and computer control is not an attempt to find a "best" solution to a well specified problem. Rather it is tailored to be able to handle the anticipated amount of data taking and computing, and otherwise to be as open and flexible as possible with respect to the ongoing and future developments of measuring modes and instrument operation. It is built around a fast PCD-60 parallel I/O interface and a Sparc 30 work station, and it is planned to allow standard interfacing with the ESO-VLTI system using VME-bus.

2.5 Data analysis

Because of unpredictable changes in the flat field of the 10 μm camera known to us (MAX), we concentrate on fringe analysis by optical path length scanning with an amplitude of λ to a few λ. This is similar to the analysis used in the Mark III optical interferometer on Mount Wilson (Shao et al. A&A **193**, 357, 1988). In addition, Fourier (speckle) techniques will be considered.

2.6 Tests

We think it necessary to have the mid-interferometric instrument operational before going to Paranal. The main tests envisaged to achieve this goal are

– 10 μm observations with the camera MAX on UKIRT to confirm the sensitivity estimates and to obtain - hopefully realistic - examples of data,

– laboratory experiments with a Mach-Zehnder interferometer setup to test optical components , data taking modes and the integrated interferometric instrument,

– instrument setup and preliminary commissioning on Paranal with the help of siderostats of sufficient size.

2.7 Interfaces with ESO

At present, the main points of interaction are

– our request to provide siderostats of sufficient size ($>$ 20 cm diameter; 20 cm being the **bare** minimum, and as such probably very inefficient, costly and time consuming),

– our need for synchronous chopping and nodding of the telescopes involved in the interferometric measurement, in order to calibrate photometrically the observed fringe amplitudes,

– the clarification of what actually the input beams into the "MIDI" instrument will be for different kinds of sources. We recommend that ESO initiate and harmonise the necessary discussions, including the question whether some functions (e.g. beam compression) should be performed centrally, once for all of the interferometric instruments.

2.8 Schedule

Internally to the Max-Planck-Institut für Astronomie the project started on June 9 of this year with the nomination of Uwe Graser as project manager and Christoph Leinert as project scientist. The first money for this project is being spent in 1997. At present, we plan to ship the mid-interferometric instrument to Paranal at the end of the year 2000.

2.9 Needed manpower, costs, resources

We estimate that a total of 15 manyears will be necessary to develop the mid-infrared interferometric instrument in the version describef in this report.

The total costs are estimated to about 1.5 million DM. This cost estimate does not include spares, nor does it include travel costs to Paranal for testing, commissioning or observing with the instrument. We assume that ESO will be taking over these travel costs.

Apart from the Max-Plamck-Institut für Astronomie the following institutions have indicated that they could contribute to the project:

– the dutch participants, if their application for a larger grant for participation in the VLTI will be successful. This will be decided before May 1998.

– the Kiepenheuer Institut für Sonnenphysik in Freiburg with manpower and monetary contributions from its annual budget.

– Meudon Observatory with manpower and a planned financial contribution of the order of 150 000.- DM. The emphasis for the contributions is on the topics of internal delay lines, spatial filtering and data analysis software.

– the Landessternwarte Thüringen with manpower only.

2.10 Open problems

This list gives the status, as of today and not necessarily complete.

– specification of the input beams

– properties of beam splitters/ beam combiners

- antireflex coatings for KRS5 or other materials transmitting from 8 μm to 26 μm
- influence of diffraction on thermal background
- alignment procedure, including mechanical alignment with the output pupils of the VLTI
- inclusion of third and fourth telescope beams
- interferometric verification of the instrument
- implications of different beam diameters from UTs and ATs
- inclusion of the 20 μm measurements; simultaneous measurements?
- verification of sensitivity and limiting magnitude
- metrology; tying "MIDI" to the other VLTI instruments and to the fringe tracker; the assumption is that ESO will provide the necesssary metrology beams.
- effectiveness of the closed cycle cooler
- mechanical disturbance introduced by the closed-cycle cooler

Part of these questions is presently under active investigation. In our opinion this list of open problems allows us to be confident that we will be able to provide a functioning mid-infrared interferometric instrument for the VLTI.

Chapter 3

Main characteristics of the instrument

3.1 Basic parameters

Wavelength coverage		10 μm band (8 μm - 13 μm)
	expandable to	20 μm band (17 μ - 26 μm)
Field of view		$\pm$ 1″ (for object acquisition)
Airy disk UTs	at 10 μm	0.26″ (for measuring)
ATs	at 10 μm	1.14″ (for measuring)
Coherence time	at 10 μm	100 ms (for fringe measurement, fringe motion $\leq$ 1 μm)
Atmospheric OPD jitter	rms	22 μm (at 10 μm)
	p-p	66 μm (at 10 μm)
Differential dispersion	in 100m of air	0.9 μm (10 μm to 20 μm)
		46 μm (1.6 μm to 10 μm)
Atmospheric stability	for chopping	200 ms
Input beam diameter	from UTs	80 mm
	from ATs	18 mm
Pixel size	of detector	50 μm
Limiting magnitude UTs	at 10 μm	5.0 mag (low accuracy mode)
ATs	at 10 μm	1.8 mag (low accuracy mode)

3.2 Observing modes and measuring modes

For easy reference, these modes are shortly repeated here from the document presented at the ISAC meeting of July 15, 1997.

3.2.1 Observing modes

This refers to the methods to determine the fringe contrast.

- *"shift and add" mode*: a fringe measurement is possible within the coherence time of 100 ms. In this bright source mode, the instrument could in principle track the fringes by its own.

- *"speckle" mode*: power spectrum averaging over many individual short (100 ms) exposures should recover a range of fringe signals which are too weak to be found in the "shift and add" method.

- *"blind integration"* or *"fringe stabilised" mode*: for this faint source mode the fringes have to be stabilised externally (by a fringe tracker or by one of the other instruments), and it has to be assured that the fringes will be stabilised also inside the instrument. Then the individual short exposures can be averaged coherently by stacking the exposures. This is the most sensitive mode of the instrument.
  Internally in the instrument, if simultaneous 10 μm and 20 μm measurements are possible, then e.g. the 10 μm channel could be used to stabilise the fringes for the 20 μm measurement. The atmospheric dispersion is small enough (0.9 μm over 100 m of air between 10 μm and 20 μm) to allow simultaneous measurements in these wavelength bands.

3.2.2 Measuring modes

This refers to calibrating the fringe amplitudes in terms of visibilities, and it requires to measure the total flux of the source (as opposed to the correlated flux giving the fringe amplitude). The total flux measurement requires the usual infrared techniques of chopping and nodding with the telescopes. This helps over the difficulties that the mid-infrared detector array flat fields are non-linear, load dependent and variable with time.

- "*unfiltered" mode:* the measurement of fringe amplitude is continued for a while (a few minutes), then the next few minutes are used for a determination of the flux of the source. This sequence is repeated as necessary. No spatial filtering is applied to the beams before beam combination. In this mode, fringe recovery is necessary only once every 10 minutes or so. Visibilities are calculated from the averages on correlated and uncorrelated flux. The resulting accuracy in visibility is estimated to be 5% - 10%.

- "*filtered" mode:* to reduce the phase fluctuations in the beams, a spatial filter is introduced into each beam before beam combination. The fringe signal is measured for one coherence time only. Chopping allows to measure the background flux during the following coherence time, and this sequence is repeated many times. It may be necessary to recover or

even find the fringes again after each chopping. In this mode, it is again the combined flux of the two beams which is measured. Visibility is calculated by applying a correction for the varying flux entering through the spatial filters on the basis of this combined flux. The resulting accuracy is estimated to be a few percent.

– "*filtered and referenced" mode:* similar to the "filtered" mode, but after the spatial filter and before beam combination part of the light in each beam is extracted for separate photometry. The visibility measurements then are corrected for the varying flux through the spatial filters on the basis of the individual flux measurements per beam. This allows to evaluate the geometrical mean of the individual fluxes, which is needed for the true correction. The resulting accuracy in visibility is estimated to be $\approx 1\%$. (At 2 μm, with the corresponding mode at the IOTA interferometer, even 0.3% have been reached occasionally).

3.3 Source finding

We consider having an imaging mode, with the beam suitably attenuated in the cold, to find the source and to center it on the detector array. For this mode, the grism is removed from the optical path. Chopping is required.

For faint sources blind acquisitions with the offsets obtained on a nearby brighter source will be applied.

3.4 Fringe finding

3.4.1 Active fringe finding

In the instrument slow changes of the optical path difference (OPD) within a range of about 1 cm are foreseen. Such a wide range for the adjustment of the optical path difference is considered necessary for the initial setup of the instrument. It also allows to explore a safe range of OPD when searching for the fringes at the beginning of a night.

3.4.2 Adaptive fringe finding

A suitable method has to be established based on the actual performance of the instrument. One possibility would be to scan a range of $\approx$ 100 μm of optical path difference (OPD), which is larger than the expected peak-to peak range of fringe motion ($\approx$ 60 μm). Therefore the fringes, if present in this range, would not leave it during the search scan. This search scan should be performed at the nominal speed used for measurements, namely 100 ms per OPD change of 10 μm. During each 10 μm interval of OPD we would be looking for the white light fringe. The full scan will last longer than the coherence time, but the fringe crossing time will be less. With real-time data processing appearance of the fringe within one of the 10 μm OPD subunits can be recognised within the order of a coherence time. Then the fringe has not yet moved by more than one tenth or two tenths of a wavelength since the detection. The search scan can be interrrupted, and

with one or two iterations on a shorter scan window the appropriate experiment-internal setting of the OPD can be determined.

3.4.3 Fringe recovery

An exploratory modulation cycle after each chopping during an interferometric measurement to verify that the fringe signal is still present. If not, fringe finding has to be done.

3.4.4 Fringe tracking, "Shift-and-add"

This is the observing mode for bright sources. The fringe signal from the source itself is used to keep the fringes within the modulation range of 10 μm to 20 μm OPD. The fringe signals subsequently can be added in phase to improve the signal-to noise ratio.

3.5 Alignment and calibration

3.5.1 Alignment

With progress on the optical design we will determine the components to be aligned and procedures to actually perform the alignment. Alignment will be part of the laboratory tests.

3.5.2 Fringe amplitude calibration

We plan to measure the modulation transfer efficiency of the instrument for interference fringes by sending in light backwards from one arm behind the beam combiner. After retroreflection at the entrance of the instrument, the modulation of the interferometric signal is to be measured in the other interferometric output.

3.5.3 Visibility calibration

Internally by photometry of the astronomical source being measured.
Externally by the measurement of calibrators (sources with known visibility).

3.5.4 Tying in with other VLTI instruments

This requires moderate accuracy metrology ($\pm$ 1 μm) and has to be discussed and defined. It can considerably enhance the sensitivity of the mid-infrared interferometric instrument and can allow to use phase referencing for the phase measurements.

3.6 Distribution of the signal on the detector

We assume a readout frequency of the detector of once every 25 ms, as used for the estimates of limiting magnitude on pages 32/33 of the July report to ISAC.

Then we expect a background signal at 10 μm of 1.5×10^9 photoelectrons per Airy disk per readout. The shot noise of this signal is larger than the signal expected from a 100 Jy source. The instrument therefore appears safely background limited in almost all cases.

However, the expected well capacity of the 10 μm array detectors is not larger than 1.5×10^7 electrons. We assume that this capacity should not be used to more than $\approx$ 50 % in order to avoid unlinearity effects. This leaves us with a usable well capacity of about 8×10^6 electrons per pixel per readout. We have to spread the signal over $\approx$ 200 pixels because of the limited pixel capacity. This spreading will be done by spectral dispersion. The long dimension of the SBRC array detector is 320 pixels. If we assume that 90 % of the light of an Airy disk are imaged on one pixel, and that this light is spectrally dispersed over the long dimension of this chip, then 4.7×10^6 background electrons per pixel per readout result. The readout noise of the detector then increases the total noise by 10 %.

This is acceptable, but the example shows that we are close to the situation where readout noise starts being important. Imperfections in the instrument may distribute the flux from an Airy disk over more pixels than anticipated, increasing the importance of read noise. And if we extract photometric beams before beam combination, putting 20 % or less into the photometric channel, then these photometric signals already will be dominated by read noise. Improvements in the read noise of the available 10 μm detectors therefore would help the instrument and definitely are wanted.

Chapter 4

Optical design

4.1 General concept

The MIDI imaging optics is built up as far as possible by reflective components to make sure that the whole wavelength band from 5 μm to 25 μm will be available without the need of exchanging intermediate imaging components. The only dioptrical imaging components are the camera systems themselves which provide the short focal length imaging of the combined collimated beams onto the detector (see Figs. 4.1-4.4). The entrance pupils of 80 mm diameter are provided by the telescope system. They are separated horizontally by 100mm. These pupils are reduced in a first step by a factor of 8 for both beams to be combined. The following delay line is realized by four flat reflections. Directly after the delay lines the beam is entering the cryostat. Thus, the following optics is cooled to cryogenic temperatures of about 70K.

An off-axis paraboloid will image the telescope focus into the first image plane of MIDI, where spatial filtering by pinholes can be provided. In order to create the space necessary to introduce a piece of monomode fiber for spatial filtering, an elliptical or toroidal mirror provides a second image plane nearby, which is identical to the first one concerning the image scale. An off-axis paraboloid re-collimates the beam. After the second paraboloid there is some space to insert a wavelength beam-splitter to provide in parallel a 10μm and a 20μm channel. At present, we propose one single channel, the optical components of which can be exchanged to switch from one to the other wavelength band. In place of the optional dichroic mirror a solid gold mirror (45°) is used.

The following beam combiner provides two combined beams, both of which will penetrate the same grism and camera system The camera will provide two combined beam images on the same detector.

For both beams a $\approx$ 20% photometric beam can be separated before the two beams are combined. They are also imaged onto the same detector.

An overview of the main optical parameters of the imaging system is given in Tab. 4.1

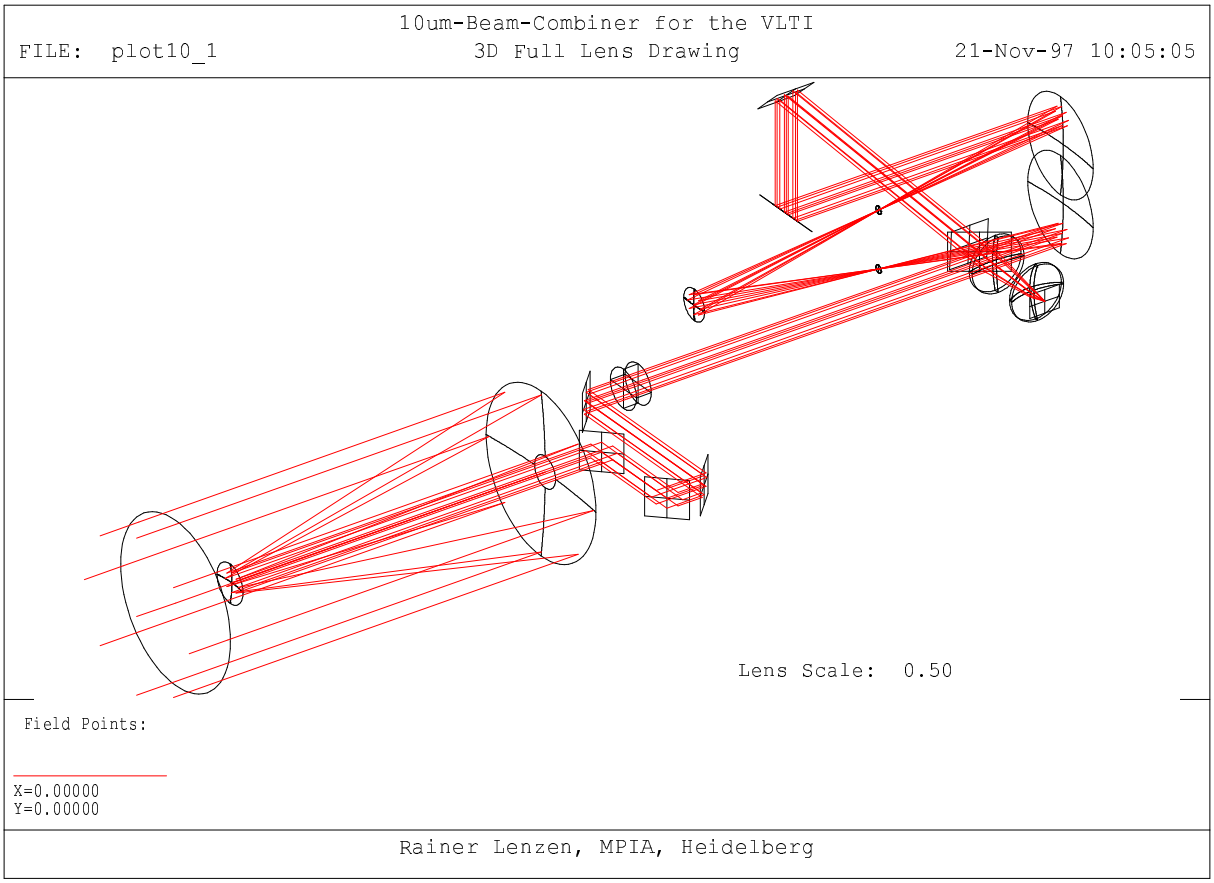

Figure 4.1: Three-dimensional representation of one of the two interfering beams. The beam combiner is the upper one of the two flat reflecting elements left of the paraboloids.

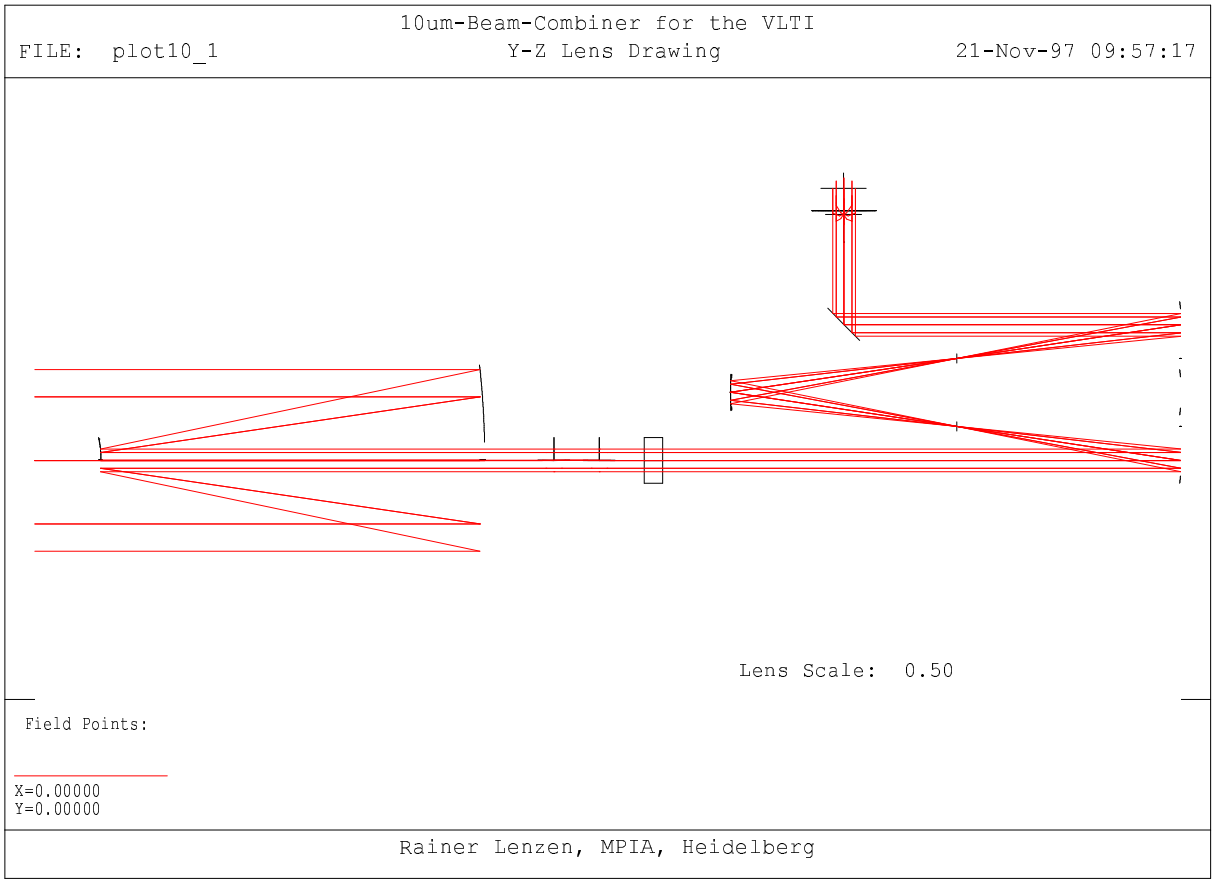

Figure 4.2: Side view representation of one beam. The beam combiner is where the upward going beam seemingly ends. The detector position is indicated by the cross.

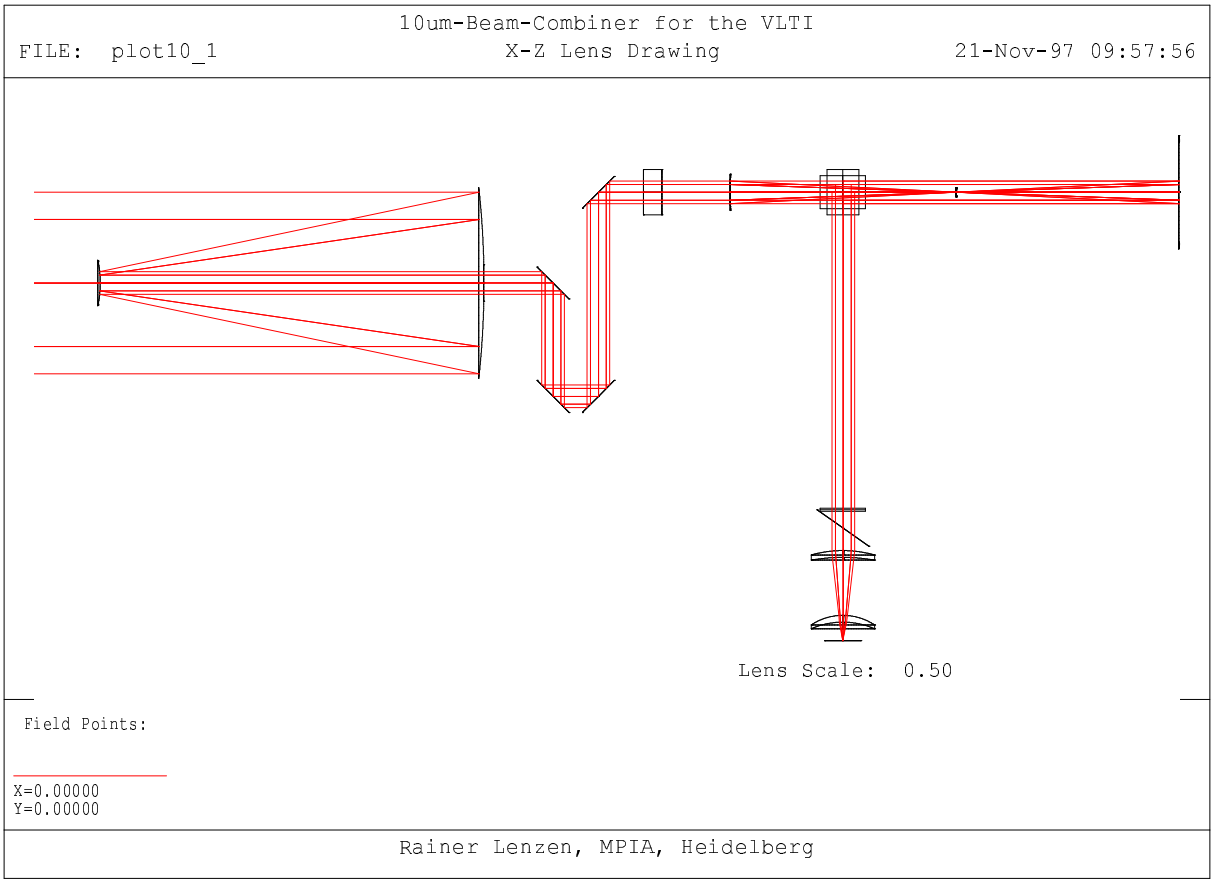

Figure 4.3: Top-view representation of one beam. The beam combiner is right of upper center, where the two rectangles overlap.

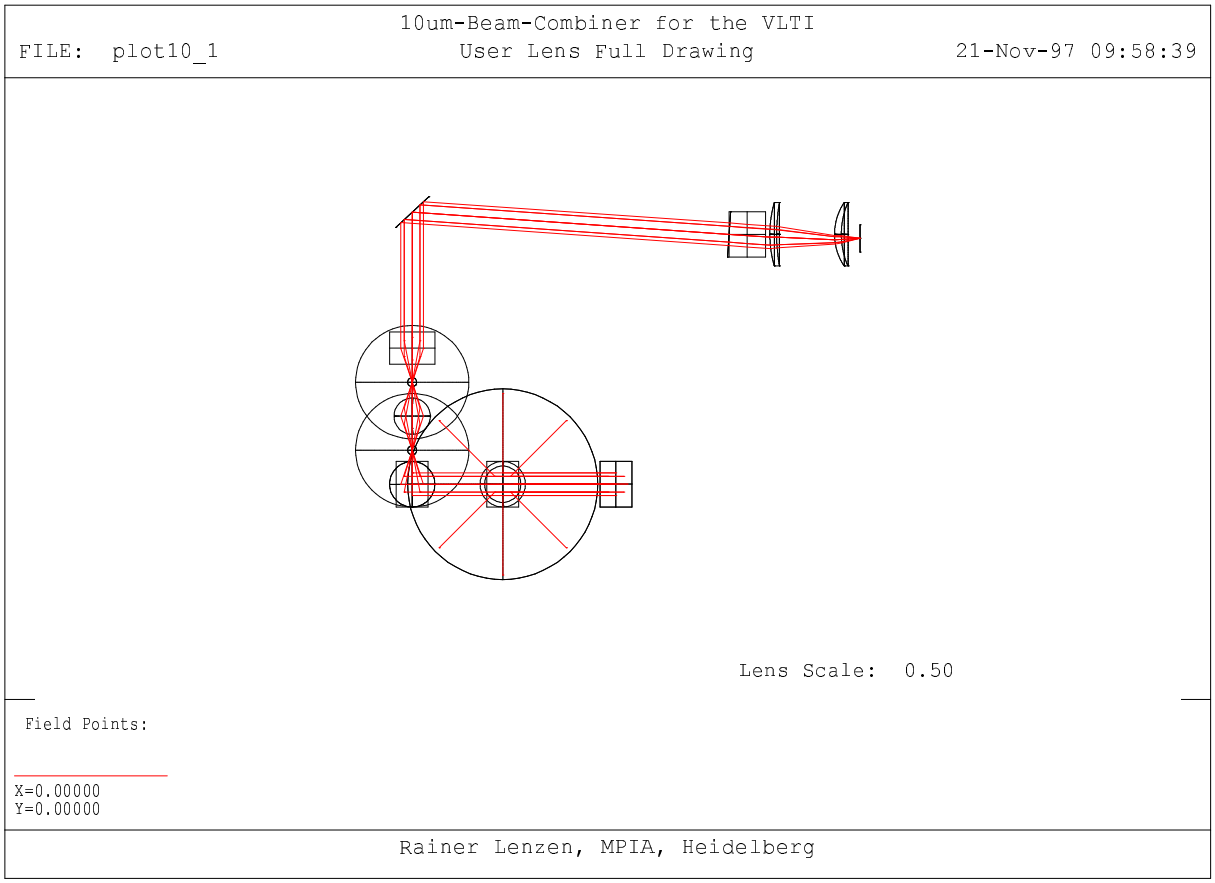

Figure 4.4: Front-view representation of one beam. The beam combiner is at upper left, the detector at upper right.

Table 4.1: Main parameters of the imaging Optics (Grism included)

Input Pupil Diameter:	80 mm
Separation of Input pupils:	100 mm
Reductor:	factor 1/8, Cassegrain System
Delay line:	160 mm, 4 mirrors
Entrance window:	10 mm KRS-5
First paraboloid	f = 100 mm
scale first focus:	f/10, 2.58 arcsec/mm
FWHM of 10 μm diffraction:	100 μm
Ellipsoid or toroid:	1:1
Second paraboloid	identical to first one
Beam splitter	10 μm and 20 μm in parallel or alternatively
Beam combiner:	10 μm and 20 μm in parallel or alternatively
Grism	33.2° KRS-5, 37.5 lines/mm second order: 8–13 μm, first oder: 16–26 μm resolution: 443 per pixel
Cameras	10 μm: 2 lenses Ge, 20 μm: 2 lenses KRS-5
Image scale:	f = 25 mm, f/2.5, FWHM airy disk: 25 μm(10 μm)
Total focal length:	200 mm

4.2 Imaging quality

4.2.1 The intermediate foci

Two intermediate foci are available: Pinholes or a fiber-link can be used to clean the beams to allow a more accurate measurement of the visibilities. The image quality for the two foci is presented by Figures 4.5, 4.6, 4.7 and 4.8.

4.3 Design of the camera system

Both for the 10 μm and the 20 μm window a camera system has been designed that fulfils our requirements. The effective focal length is 25 mm and the minimum Strehl ratio is about 80%.

To obtain this image quality even for spectroscopic application up to the edges of the detector, at least two lenses are necessary. Here we concentrate on the 10 μm band. The camera for this wavelength region is built up by two Germanium lenses (see Fig. 4.9) which can be antireflex-coated up to a high degree of transmission (better than 98% per lens). A possible solution for the 20 μm region (not shown here) could be built up from two KRS-5 lenses of similar shape.

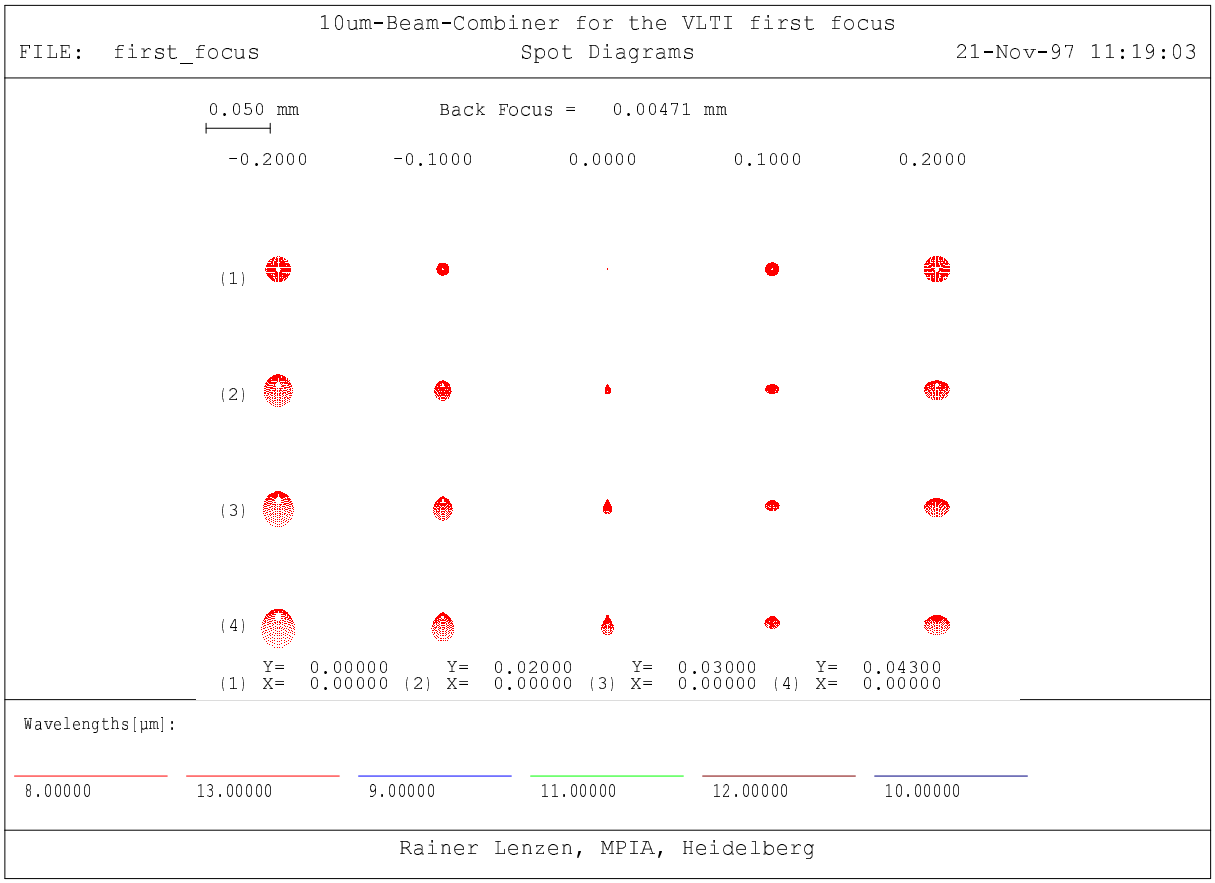

Figure 4.5: Spot diagram at the first focus on axis and for three field angles up to the edge of the FOV. From left to right: five focus positions, see values in mm given on top of the diagram. From top to bottom: four field angles, given as "Y" below the diagram in degrees, and corresponding to 0″, ± 0.72″, ± 1.08″ and ± 1.55″ on the sky.

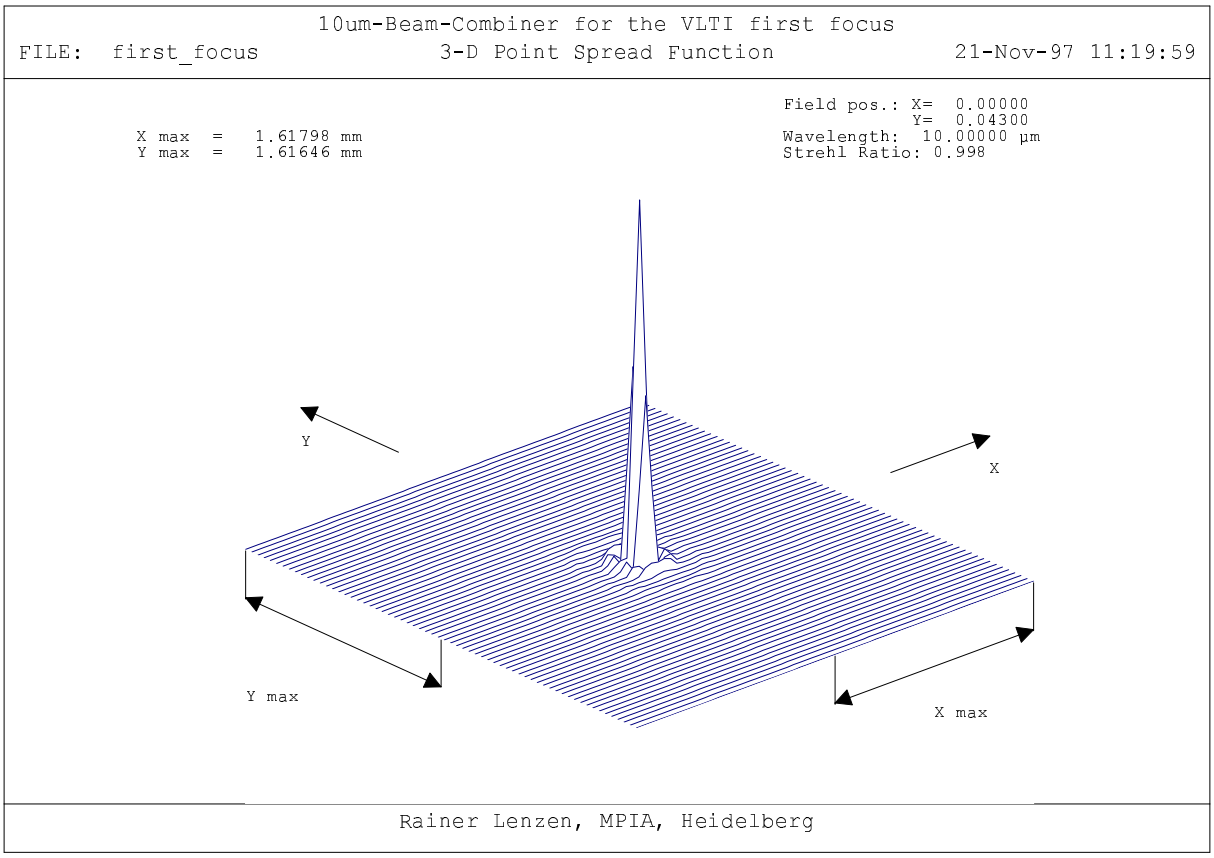

Figure 4.6: Point spread function at the first focus for an extreme field position at the edge of the $\pm$ 1.5″ FOV.

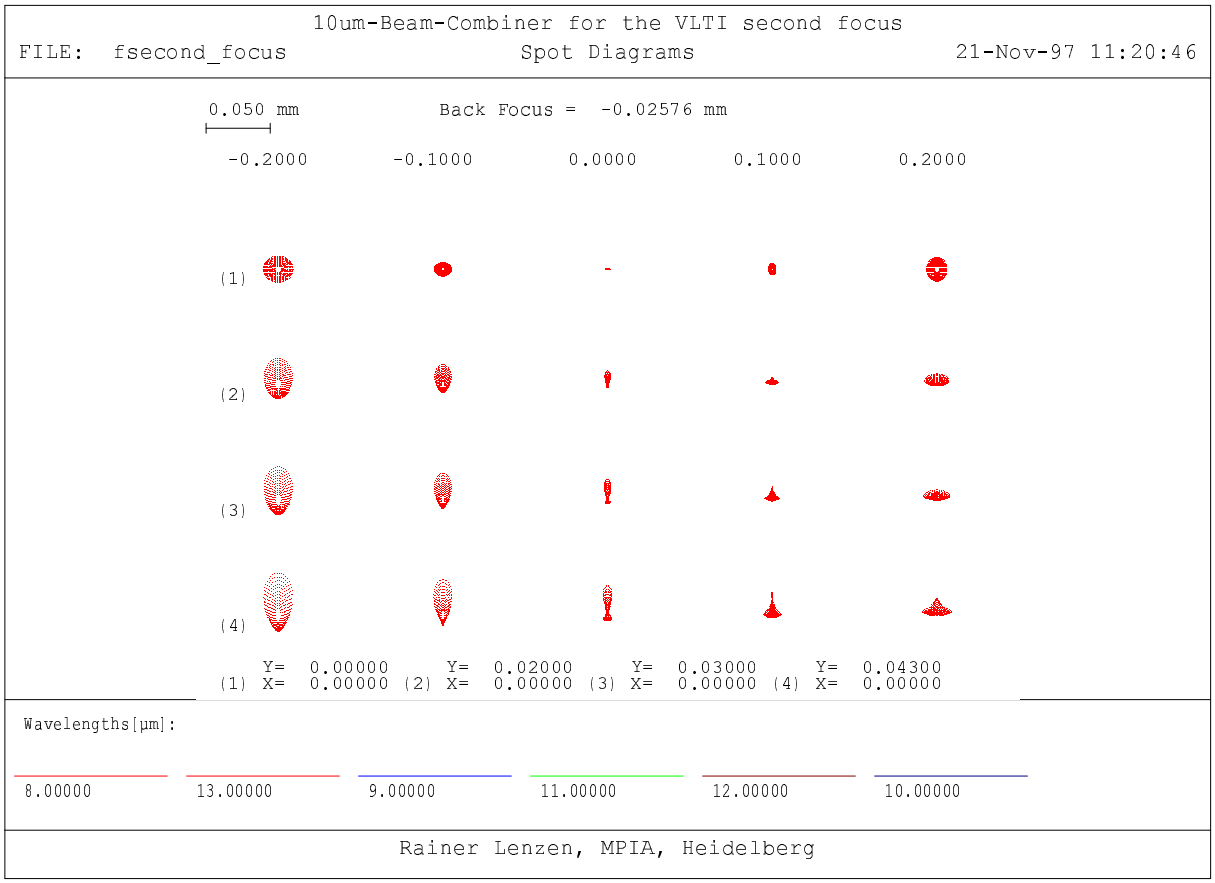

Figure 4.7: Spot diagram at the second focus on axis and for three field angles up to the edge of the FOV. From left to right: five focus positions, see values in mm given on top of the diagram. From top to bottom: four field angles, given as "Y" below the diagram in degrees, and corresponding to $0''$, $\pm$ $0.72''$, $\pm$ $1.08''$ and $\pm$ $1.55''$ on the sky.

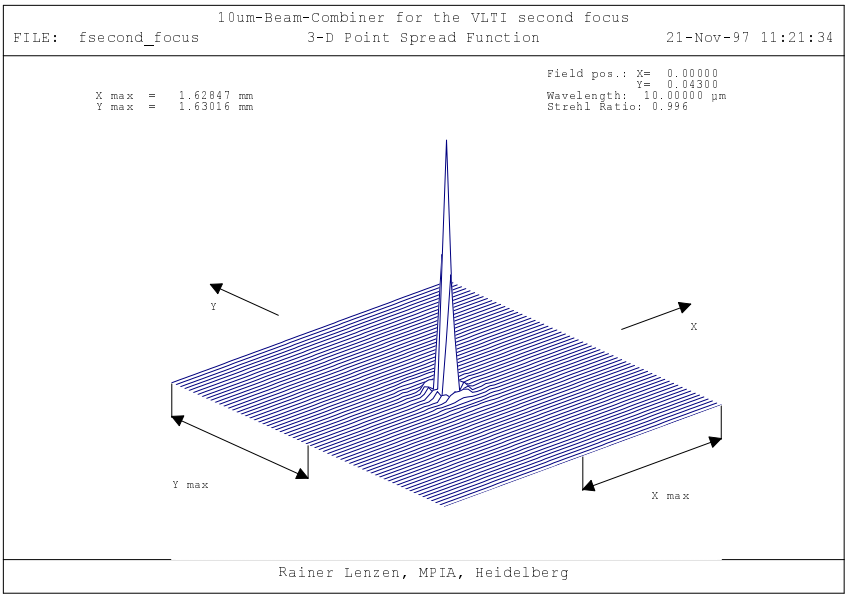

Figure 4.8: Point spread function at the second focus for an extreme field position at the edge of the $\pm$ 1.55″ FOV.

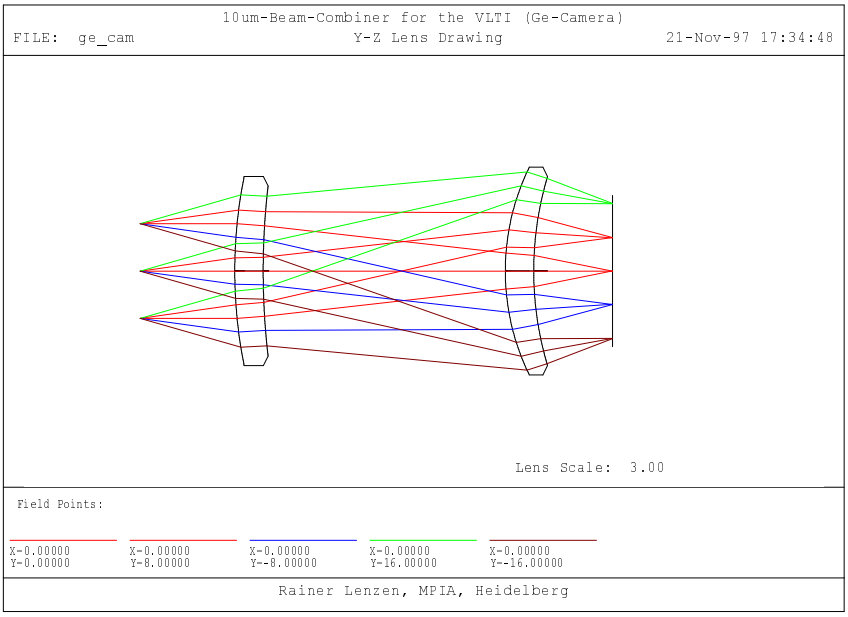

Figure 4.9: Design of the Germanium lens system for the 10 μm band

Table 4.2: Strehl ratio of the complete optical system of MIDI for several off axis angles and Wavelengths

off axis [°]	off axis [″ on the sky]	**Wavelengths [μm]** 8	9	10	11	12	13
0.00	0.00	0.956	0.955	0.957	0.960	0.963	0.966
0.20	0.72	0.860	0.884	0.902	0.916	0.927	0.936
0.30	1.08	0.882	0.861	0.838	0.836	0.860	0.846
0.43	1.55	0.788	0.820	0.957	0.950	0.846	0.839

Table 4.3: Overall transmission of the imaging system of MIDI without grism. For the grism a maximum transmission of about 60 % is expected.

Component	material	single refl.	number	tot. refl.
Cass. reducer	gold	99.4	2	98.8
ODL	gold	99.4	4	97.6
Window	CdTe	98.0	1	98.0
re-imaging	gold	99.4	3	98.2
Band selection	gold	99.4	1	99.4
combiner	dichroic	95.0	1	94.0
camera	Ge AR	98.5	2	97.0
Total				84.1

4.3.1 The detector focus

The image quality is given in the following figures in form of a spot diagram (4.10) and as three-dimensional point-spread functions, which give the corresponding Strehl-ratio as well (4.11-4.14) Assuming a detector pixel size of 50μm, for all field positions and wavelengths more than 80% of a point source intensity is imaged onto one pixel due to the fact that a f/2.5 camera is used and the approximate FWHM of the Airy disk (= $\lambda \times$(F-number N)) equals half a pixel. The calculated Strehl ratios are given in Tab. 4.2 for several wavelengths and off-axis angles.

4.3.2 The overall transmission

The overall transmission of MIDI is defined by the reflectivity of gold (10 mirrors: Cassegrain reductor, optical delay line, re-imaging system and one 45° folding mirror), the entrance window, the beam combiner and the camera system. In addition, in general the grism is used. In Tab. 4.3 the single contributions are combined to a total transmission of 84.1% without grism. Following experimental experiences with directly rooled KRS-5 grisms a maximum transmission of about 60% is expected.

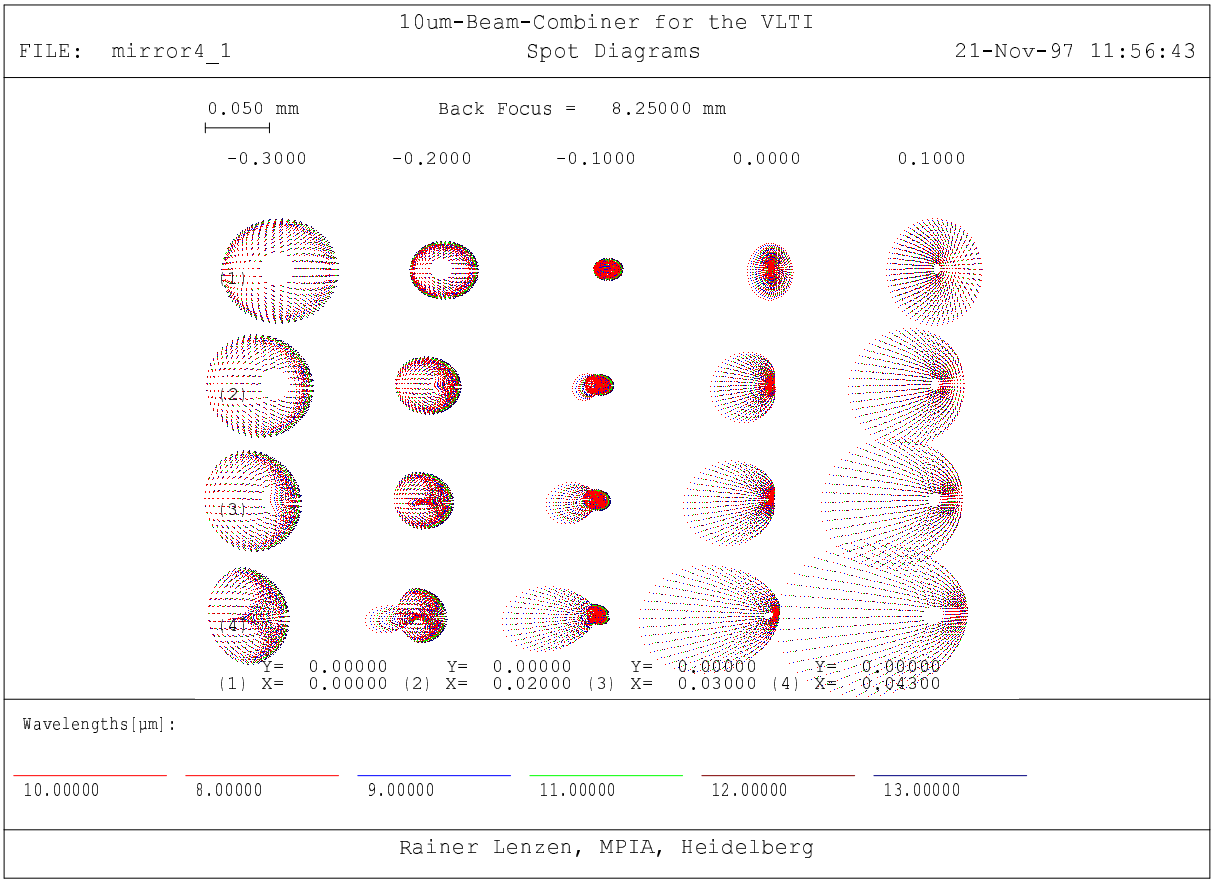

Figure 4.10: Spot diagram of the detector focus for several wavelengths, field positions, and off-focus positions. Focus positions are given from left to right as indicated by the line above the diagram in mm. Field angles are given from top to bottom as indicated in the line labeled "Y" below the diagram in degrees. They correspond to 0″, ± 0.72″, ± 1.08″ and ± 1.55″ on the sky. The wavelengths from 8 μm to 13 μm are coded by colour (A colour version of this plot is appended.

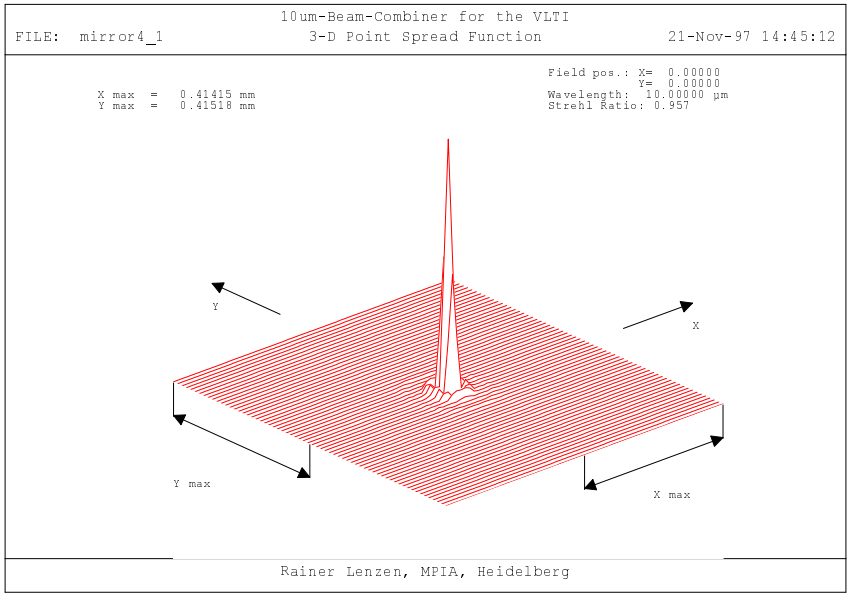

Figure 4.11: Point spread function of the whole imaging system for on axis field position.

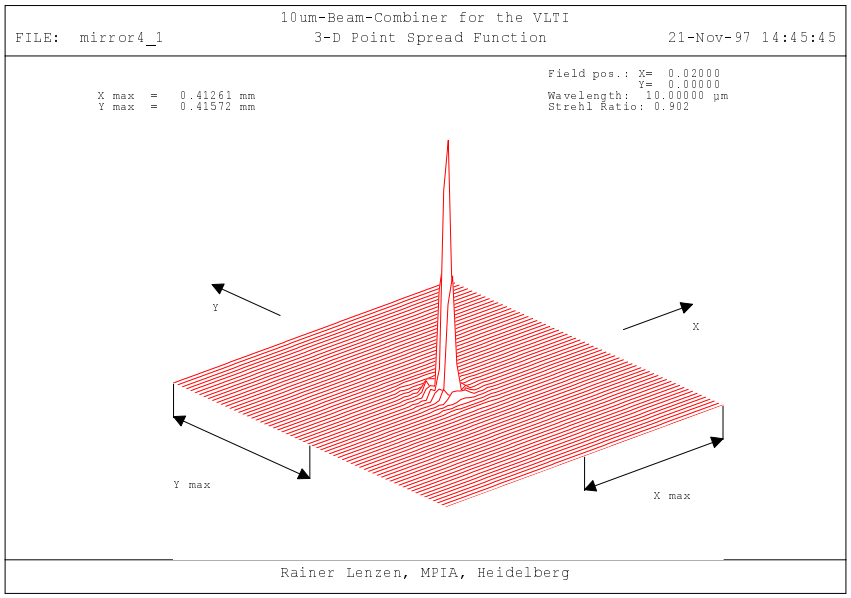

Figure 4.12: Point spread function of the whole imaging system for a field position of 0.02° (0.72″ on the sky) off center.

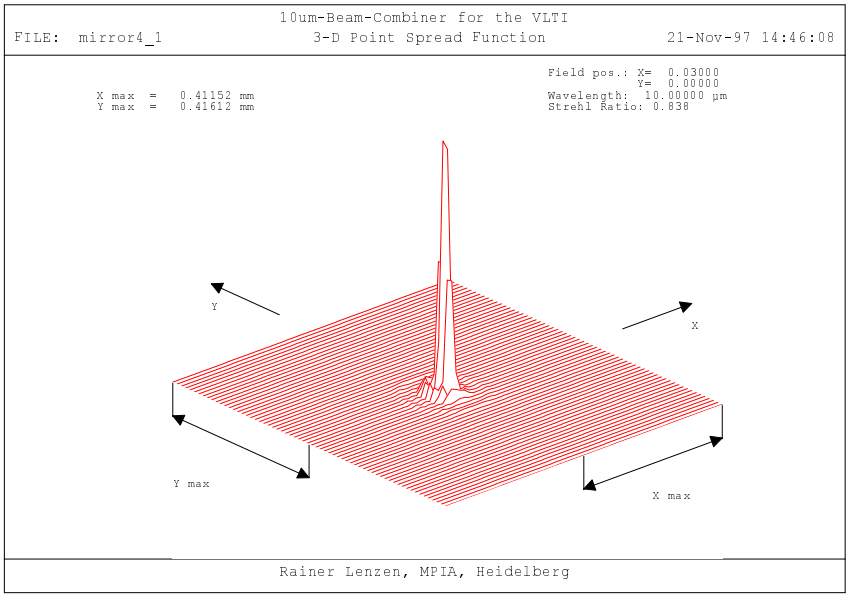

Figure 4.13: Point spread function of the whole imaging system for a field position of 0.03° (1.08″ on the sky) off center

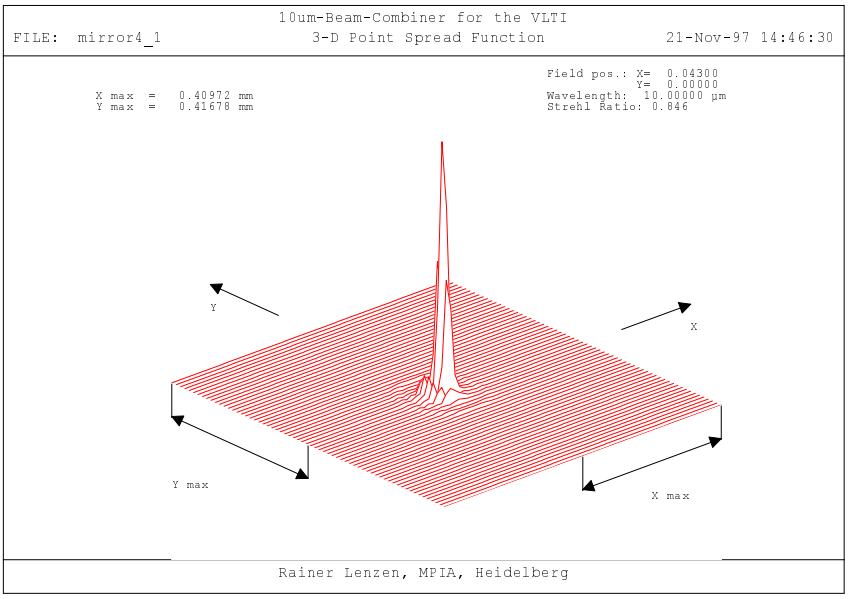

Figure 4.14: Point spread function of the whole imaging system for a field position of 0.043° off center (edge of FOV, ± 1.55″ on the sky).

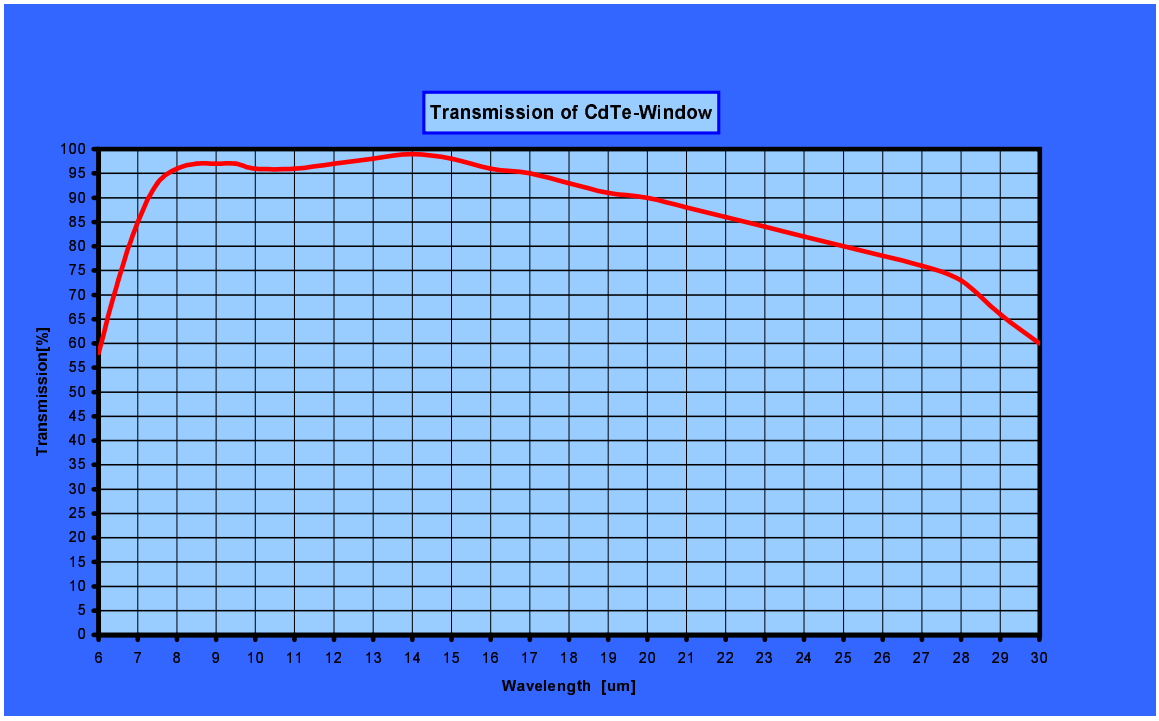

Figure 4.15: Measured transmission of antireflection-coated CdTe

4.4 The entrance window

Both beams are entering the cryostat through a common window. The beam separation is 20mm at this position, the pupil diameter is 10mm each. Thus, a window size of about 40mm x 20mm is required. The thickness may be 5mm.

Best choice for a common 10 and 20 μm window is anti-reflection coated Cadmium-Telluride a transmission measurement of which is given in Fig. 4.15. Experience with the MAX camera on UKIRT shows that because of the hygroscopic properties of the antireflex coating the window may have to be removed after each observing run for a new coating. We want to explore ways to avoid this frequent change.

4.5 The grism

The present design of the grism is driven by the idea to be able to use the same grism both for the 10 μm and 20 μm wavelength ranges. Therefore the choice of KRS-5 for the material. KRS-5 grisms can be directly ruled. With a prism angle of 33.2° and a ruling of 37.5 lines/mm one can use it for the range of 8 μm to 13 μm in second order, for the range of 16 μm to 26 μm in second order. The spectral resolution of $\approx$ 400 per pixel images the whole wavelength band into the long dimension of the detector. Based on previous experience with directly ruled KRS-5 grisms, a maximum transmission of about 60 % is expected.

4.6 Single-mode waveguides for spatial filtering at 10 μm

The following subsections report the status of monomode fibers for the 10 μm wavelength range. No definite point has been reached yet in their development. Therefore we do not rely on the availability of monomode fibers for this wavelength range in our instrument design. However, as mentioned above, we keep the design open for later inclusion of fibers, should the development of the coming few years promise substantial gains for doing so.

4.6.1 Hollow waveguides

Hollow waveguides, similar to waveguides used for radio interferometry, have been developed. These waveguides are multi-mode and no single-mode waveguide based on a similar technology is known to exist or to be under development.

4.6.2 Fiber optics

Traditionally, the Meudon interferometry group has developed and maintained constant contacts with, essentially, the French infrared single-mode fiber optics manufacturers community. Two groups are to be identified:

- The Le Verre Fluoré company who are the providers of the infrared fibers for the FLUOR experiment;
- the University of Rennes in Brittany who have conducted the fundamental research in the field of infrared fibers which led to the fluoride glass fibers.

Two different possibilities are investigated to produce single-mode fibers for the 10 μm range. The first one is based on the use of halogenides (e.g. KBr, NaCl, KCL). These materials have the required transmission but they are deliquescent. Building fibers with these materials would require heavy R&D investments (a few million FFRs). The alternative solution is to use chalcogenides which, in turn, are stable. Some multimode fibers made of As2Se3 or Te4Se10As5I have been produced by Artichenko in Russia and by the university of Rennes. These fibers have transmissions as good as 0.5 dB/m between 7 and 9 μm. A collaboration has been initiated between the Meudon interferometry group and the university of Rennes to produce single-mode

fibers for the M and N band with chalcogenides by mid-1998. These fibers will be tested on the IOTA interferometer (extension of the FLUOR experiment to the thermal IR).

No single-mode X-couplers are anticipated up today for the N band.

The Meudon interferometry group is also considering the possibility to purchase single-mode couplers for the 5 μm range. These couplers would be made of a fluoride glass (InF3) with a transmission of 1dB/m and would be provided by Le Verre Fluoré.

4.6.3 Integrated waveguides

The group of the university of Rennes has demonstrated the feasibility of integrated optics with fluoride glass up to 7 μm. They have some ideas on how to proceed with chalcogenides to increase the optical bandpass up to 10 μm but nothing can be taken for granted since nothing has been demonstrated yet.

4.7 Beamsplitters

4.7.1 Beamsplitters and beam-combiner

The optical design of MIDI comprises one $\approx$ 20% beamsplitter for extracting beam for photometry for each incoming beam and a 50% beamsplitter to be used for beam combining.
Particular attention is devoted to the characteristics of the beam combining beamsplitter.

4.7.2 Polarization effects

A two-beam interferometer can show degraded fringe visibility arising from polarization-dependent phase shifts at mirror surfaces in the two arms of the interferometer. In order to avoid this degradation a sufficient but not necessary condition is that each beam must experience reflections with the same sequence of direction cosines between the collecting point and the point where it is combined (Traub, 1988).
ESO provides symmetric reflection paths for the beams down to the laboratory interface, so that we are only concerned about polarization effects in the beam-combining area. One of the beams must undergo a total reflection at a mirror surface plus a partial transmission at the beamsplitter, while the other undergoes only a partial reflection at the beamsplitter.
The first beam will be affected by a phase shift $\Delta(p-s)_{\alpha,1}$ for the mirror reflection and $\Delta(p-s)_{\beta,1}$ for the partial transmission, while the second beam will suffer a phase shift $\Delta(p-s)_{\beta,2}$ due to the partial reflection. The differential retardation between the phase of the two beams is given by

$$\Delta\Phi = \Delta(p-s)_{\alpha,1} + \Delta(p-s)_{\beta,1} - \Delta(p-s)_{\beta,2}$$

which can be written

$$\Delta\Phi = \Delta\alpha_p - \Delta\alpha_s + \Delta\beta_p - \Delta\beta_s$$

where $\Delta\alpha_p$ and $\Delta\alpha_s$ are the phase shifts for p- and s-polarization due to the total reflection and $\Delta\beta_p$ and $\Delta\beta_s$ are the phase shifts between the two beams for the p- and s-polarization due to the beamsplitter.
The phase retardation decreases the fringe visibility by a factor

$$V_{pol} = cos\,(\Delta\Phi/2)\,.$$

From an estimation made for the interferometer relay optics (ISAC 1997), we know that $\Delta\alpha_p - \Delta\alpha_s < 10^\circ$ at 10 μm. As far as the beamsplitter is concerned, we are actually investigating several beamsplitter coating solutions to select the one which provides the smallest phase retardation between p- and s-polarization, and at the same time nearly equal intensities for the beams after splitting (see Figure 4.16). Figure 4.17 similarly shows the phase for p- and s-polarization for the transmitted and the reflected beam respectively. As is the case for the transmission curves, these Figures show performances predicted by the manufacturer, Laser Zentrum Hannover, for an incidence angle of 45°,a ZnSe substrate and no absorption losses. The phase shift $\Delta\beta_p - \Delta\beta_s$ is $\approx 0^\circ$ at 10 μm and it increases to about 4.5° at 12μm. Even at 12 μm the degradation in fringe visibility, V_{pol}, is less than 1%. We are also investigating the properties of different material for the beamsplitter substrate. At the moment ZnSe, KCl, and KRS5 are being considered according to their transmission characteristics and index of refraction at cryogenics temperature of about 70K. A compensator plate of the same material will have to be used to account for the path variation affecting the beam which travels across the beamsplitter.
The phase shift for reflection on gold coated mirror under 45° incidence angle is estimated to be at most 2°, which is negligible.

Traub W.A. ESO Conference and Workshop Proceed. No. 29, 1988
ISAC meeting #5, 1997 SPG-VLTI - 97/004

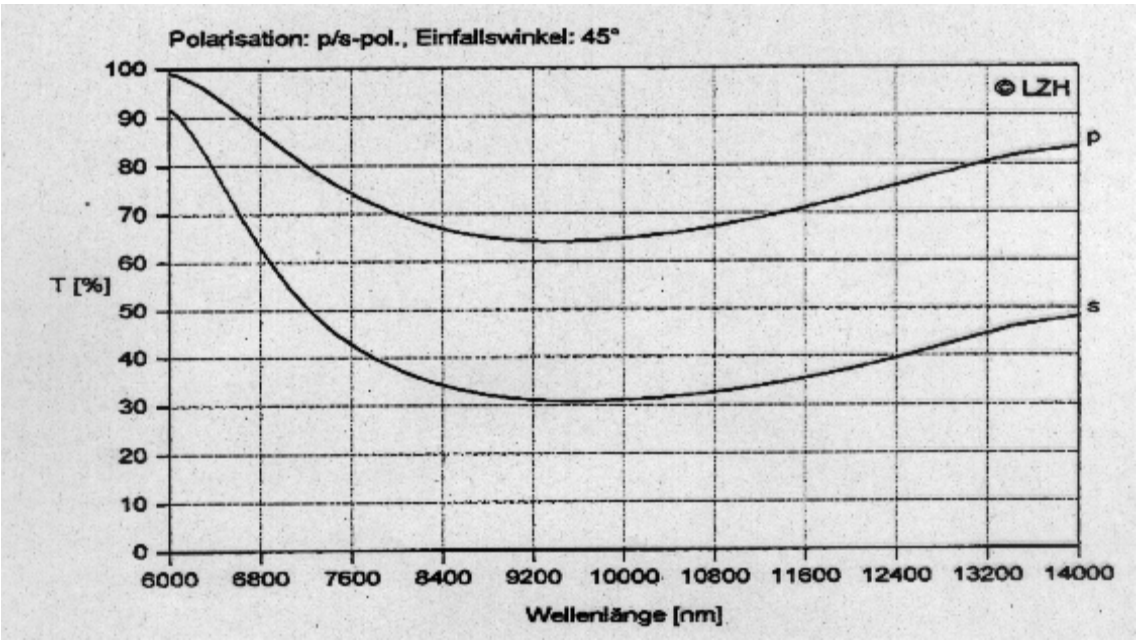

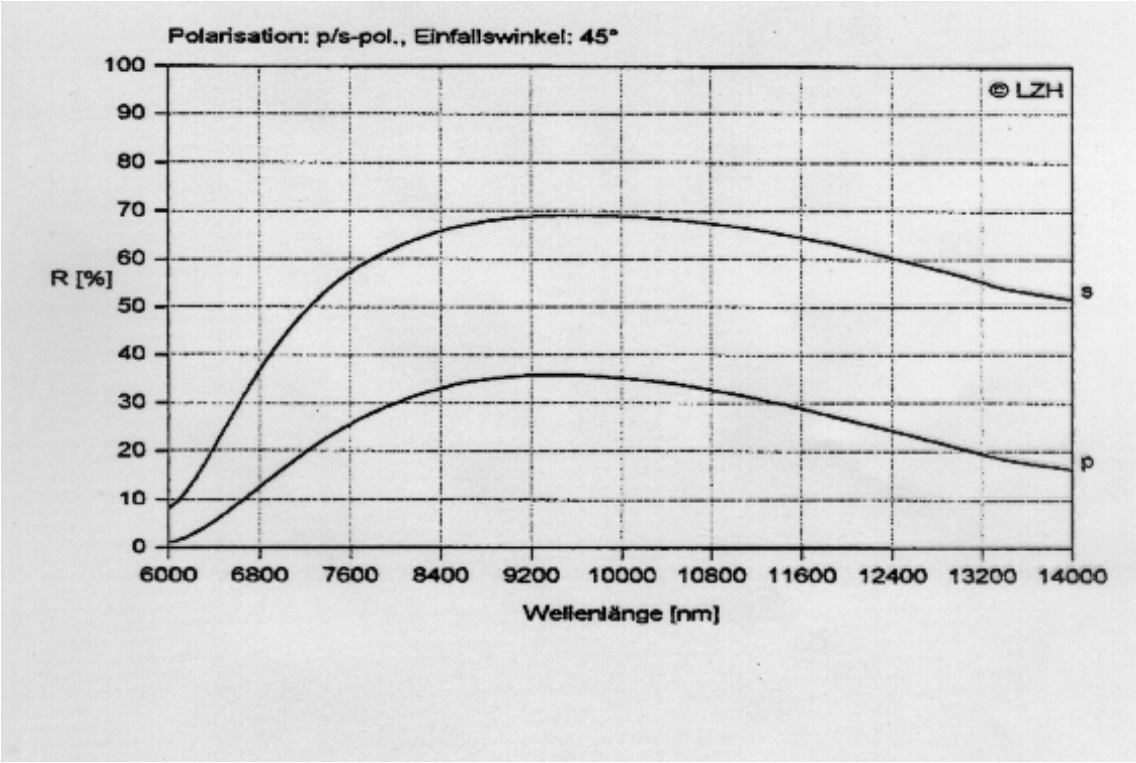

Figure 4.16: Transmission curves for the p- and s-polarisation. Upper panel:transmitted light; lower panel: reflected light. This performance has been predicted for 45° incidence angle, ZnSe subtrate, and no absorption losses by the manufacturer.

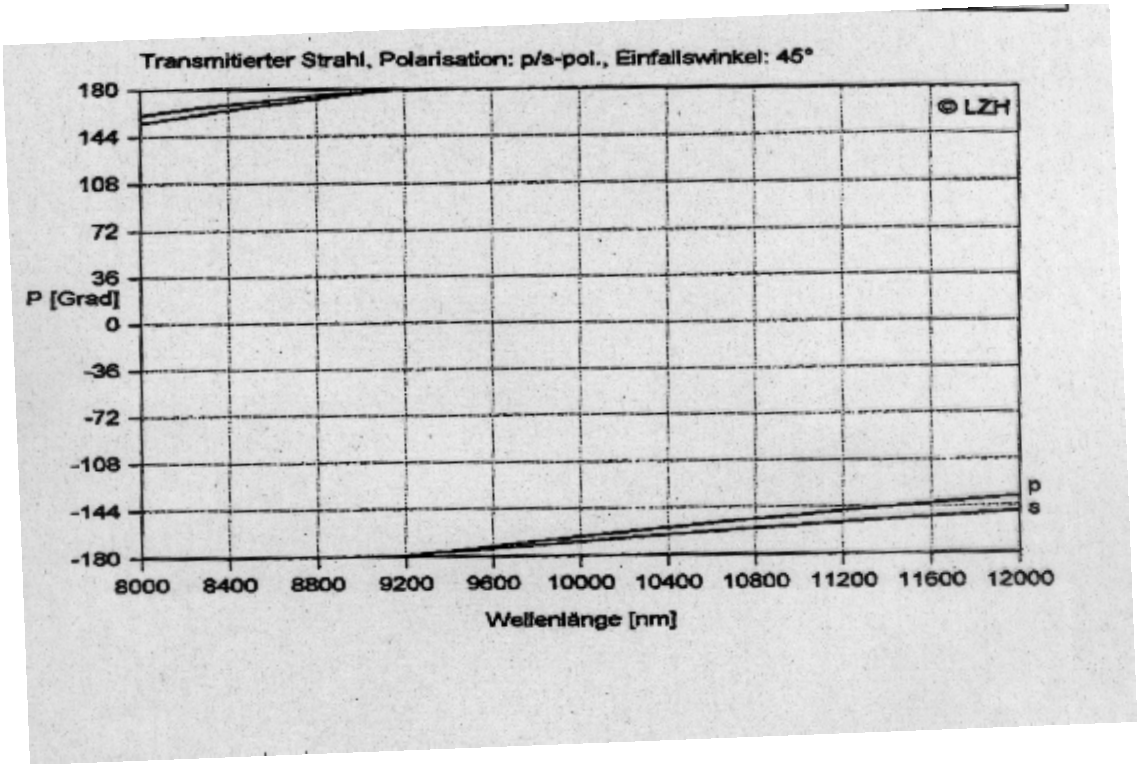

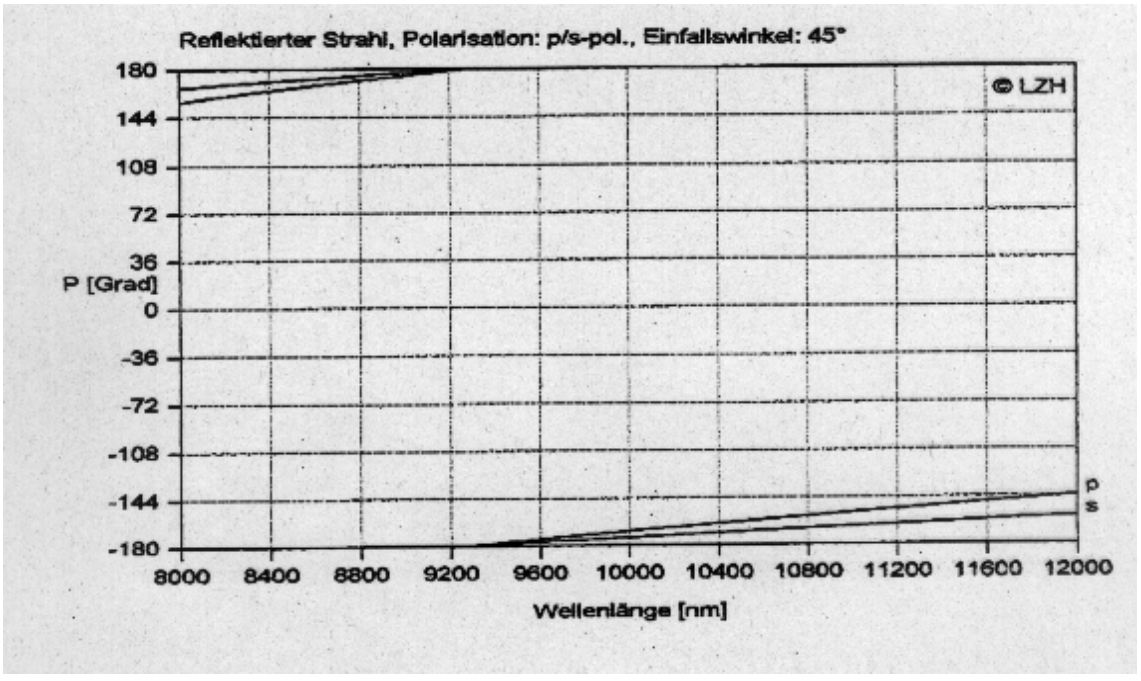

Figure 4.17: Phase for p- and s-polarization of the transmitted beam as a function of wavelength. Upper panel:transmitted light; lower panel: reflected light. This performance has been predicted for 45° incidence angle, ZnSe subtrate, and no absorption losses by the manufacturer.

Chapter 5

Detector

Since there is an ongoing development in detector technology the final selection of the detector will be postponed until 1999.
Nevertheless, the crucial requirements can be set already now.
For the following considerations it is assumed:

- The **coherence time** is 100 msec.
- The **maximum integration time** t_{int} with four OPD-steps to be scanned during the coherence time then is 25 msec.
- A **detector array** has to be used since:
  1. We want to do low resolution spectroscopy.
  2. To reduce visibility loss due to the spectral bandwidth effect to $\leq$ 1%, the spectral resolution R has to be $\geq$ 13 (for $\Delta\lambda$ = 5 μm and an OPD of 1 λ) !
     No dispersion (R=2) would decrease the visibility signal by 36% !
  3. The signal has to be spread over several pixels since the full well capacity of current detectors is too low.

  If we are background limited the signal can be spread over still more pixels without loosing accuracy. Thus we recommend to use a full line of the detector array for spectroscopic dispersion. Then the spectral resolution and the signal-to-noise ratio can be optimized by a suitable binning. If it is possible to image the Airy-disk onto one pixel size then we would end up with e.g. n = 320 pixel (or R=640, respectively) for the SBRC detector.
- Currently there are 2 detector factories that deliver (already or in the next future) suitable detectors: Rockwell and Santa Barbara Research Center (SBRC).

	Pixel No.	Pixelsize $[\mu$m$]$	Full well $[e^-]$	ReadNoise $[e^-]$	Readout channels	costs US $	availabe ?
Rockwell	128 x 128	75	2 x 10^7	1300	16	100000	yes
Rockwell	256 x 256	50	1.5 x 10^7	?	16	100000	this year (?)
SBRC	320 x 240	50	2 x 10^7	?	16/32	95000	yes

- The high **thermal background** from the 19 warm mirrors ($5 \times 10^{10}\ e^-/sec$) and the sky ($3.8 \times 10^9\ e^-/sec$) makes it necessary to spread the signal over several pixels in order not to saturate the current available detectors. Assuming a full well capacity of $1 \times 10^7\ e^-$ per Pixel the thermal background of $1.35 \times 10^9\ e^-$ per maximum integration time (t_{int}) of 25 msec requires the signal to be spread over at least 135 pixels.

- The **Readout Noise** is not negligible since with 320 Pixel the shot noise of the background is about 2000 e^- per integration time t_{int}, which is about double the Readout Noise.

- As **future developments** SBRC is planning to undertake a three-years project (together with NASA Ames and Cornell University) to develop large-format Si:As IBC arrays for an extension of the NGST to thermal IR-range.

In general, further statements in this document refer to the SBRC-device as detector.

Chapter 6

Electronics

6.1 Read-out electronics

The design for the read-out electronics to be built at MPIA is shown in Fig. 6.1. In principle all boards indicated in the drawing already have been implemented in one or the other instruments built at MPIA. Probably the clock-driver-, the pre-amplifier- and the digitization-board may need some adaptations. High data-rates as expected from our measurement modes should be no problem with this detector read-out electronics. Right nowwe are testing the high speed data link by using a SCD60 I/O interface (60 MB/sec) in a SUN-workstation.

6.2 Control electronics

There is a lot of experience at MPIA concerning the building of instrument control electronics. Figure 6.2 gives an overview on the control electronics of the instrument.
In detail, some points are still under discussion, e.g. if - or where - to use stepper motors inside the dewar or to install motors with encoders in the warm by applying feed-throughs. There will be a decision on these questions in the near future.

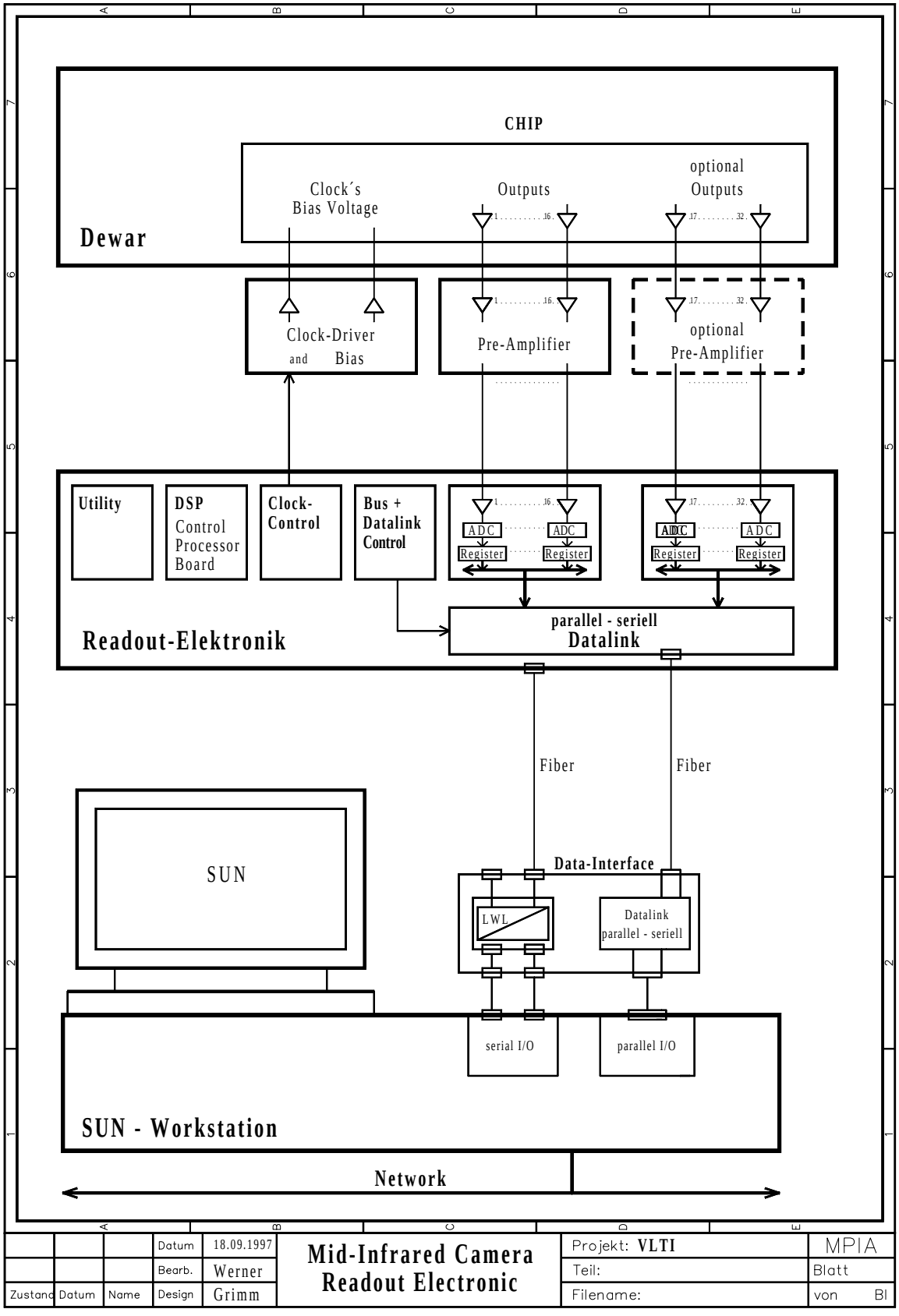

Figure 6.1: Readout electronics for the MIDI instrument.

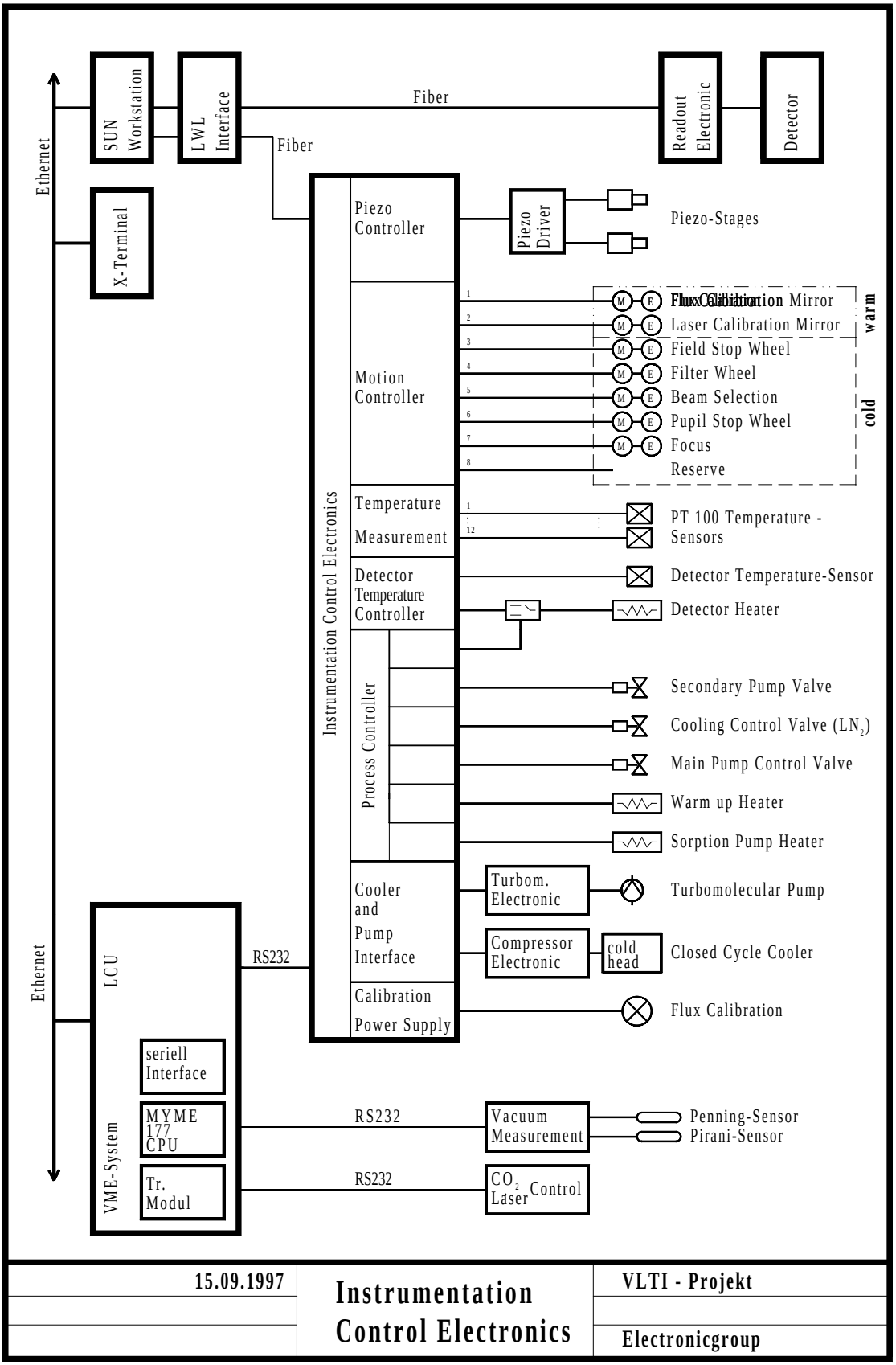

Figure 6.2: Control electronics for the MIDI instrument.

Chapter 7

Computer and instrument control

7.1 Overview

This chapter gives a rough sketch of the computing and control requirements concerning the MIDI instrument for the VLTI. The design of a control system for MIDI, the first mid-infrared camera for the ESO VLT Interferometer (VLTI), has to be as open as possible for future changes and enhancements mainly because:

- first light for MIDI is foreseen for the end of year 2000
- larger mid-infrared detectors might become available within the next years

7.2 Hardware Requirements

As with most MPIA or VLT(I) instruments a multi-platform, network-based control system is the most suitable architecture. The use of standard industry buses like the VME and PCI bus allow applications based on standard off-the-shelf interface cards.

7.3 Software Requirements

The availability of a real-time operating system (μs response time) like Tornado and a quasi real-time operating system (ms response time) with multi-user capabilities like Solaris allow all kinds of modern instrumentation (open loop and closed loop) control.

7.4 External Interface Requirements

The control hardware and software shall fit into the VLT(I) environment. This is accomplished with fast networks links (ATM, fast Ethernet, or giga-bit Ethernet) which provide the hardware communication layer among all required subsystems, e.g. communication with the telescope control system (TCS).

The VLT(I) workstation software CCS (Central Control Software) can be used as the software communication layer between MIDI and VLT(I) subsystems, e.g. communication with the TCS interface (tif). Other VLT(I) hardware or software modules can be used as necessary, e.g. the time reference system (time bus).

7.5 Control System Architecture

The proposed control system architecture for the MIDI instrument is shown in figure 7.1. This proposal can be seen as a result of the requirements given above as well as MPIA's experience with:

MAX a mid-infrared camera built at MPIA for the 3.6m UK infrared telescope (UKIRT) on Mauna Kea

OMEGA near-infrared cameras with one million pixels build at MPIA for the 3.5m telescope on Calar Alto

ALFA an adaptive optics with laser guide star system operated at the 3.5m telescope on Calar Alto

The selected hardware components like SPARC architecture with PCI-bus and Motorola 68060 architecture (master CPU inside the VME crate) with VME-bus provide enough flexibility for the future. Solaris from Sun Microsystems and Tornado from Windriver have adequate (Solaris) and excellent (Tornado) real-time capabilities.

The data flow from the MIDI detector via the readout electronics into the Sparc workstation shows only one (and currently preferred) possibility. Feeding detector data into the VME/Tornado system is also possible but only second choice. The advantage of using a Sparc workstation as detector local control unit (detector LCU) and instrument workstation (WS) in one is:

1. easy installation of 1–2 gigabyte RAM (double buffering)
2. fast (off-the-shelf) data interface available
3. real-time requirements are in the ms response time regime
4. fast data storage available
5. fast graphics adapters available (in particular for quicklook)

The detector data flow as indicated in figure 7.1 starts from the MIDI detector. For a detector with 320 by 240 pixels (e.g. SBRC Si:As (IBC)) we can assume 32 parallel readout lines and a frame rate up to 350 Hz (maximum theoretical framerate with 1 MHz ADC's: 320 x 240 / 32×10^6 = 2.4 ms/frame = 416 Hz full frame rate). The amount of data produced with the supposed maximum frame rate of 350 Hz and with an intensity resolution of 16 bit gives about 52 MByte per second.

The readout electronics has to be designed such that it can pre-process the incoming data (co-adder, background subtraction, Video signal generation, and as an option synchronization with the OPD Piezo drives) and send them (pre-processed or raw) over a fiber link to the workstation.

The proposed workstation data interface is a high speed 16-bit parallel DMA channel between the readout electronics and the workstation's PCI bus. This interface card uses direct memory access and asynchronous I/O to achieve transfer rates up to 60 MBytes per second. It uses a synchronous hardware protocol.

The serial to parallel converter is an MPIA in-house development including a loop back mode for testing.

The data management inside the workstation will be based on a double buffering scheme. Two gigabytes of memory will allow a continous data flow at the maximum detector frame rate for about 15 seconds.

Interferometric data are taken with different optical path differences (OPD) between the (two) interfering beams. The OPD can be controlled from

1. the workstation
2. the readout electronics
3. optional from the LCU

In a first attempt the workstation seems to be the most natural place to control the OPD because it is synchronized with the incoming data. The readout electronics running the clocks to drive the readout process is equally good for this task. Analyzing the incoming data while stepping through the different OPD's would allow closed-loop OPD sequences on the workstation side. Other tasks like fringe finding and tracking can only be performed with parallel access to the detector data.

The second branch of the MIDI control system is responsible for managing and operating motorized stages (filter wheels, field stops wheels tec.), the entire pump and cooling system (closed cycle cooler, vacuum pumps, etc.), calibration sources, and temperature control. All these tasks run inside the local control unit (LCU, or in MPIA "language" input/output controller (IOC)).

The LCU controls the connected hardware either directly through VME-bus interfaces or through the instrumentation control electronics. As an example, the instrumentation control electronics may be a intelligent motion control sub-system controlling 8 motorized stages. In this case the LCU would communicate with the instrumentation electronics over a serial (RS232) line. The LCU might contain interface hardware in order to access the VLT(I) time reference system.

The actual status of the entire instrument will be stored in a real-time database. Using EPICS (experimental physics and industrial control system) – the standard MPIA software package for instrumentation control – its real-time database can also directly control hardware. Reading and modifying the EPICS database is achieved through a mechanism called channel access (CA). Channel access libraries as well as executable CA programs are available for most platforms (including Solaris, HPUX, and Tornado). Tcl/Tk, IDL, and perl should be named in this context which allow a CA based communication with the EPICS database running inside the LCU.

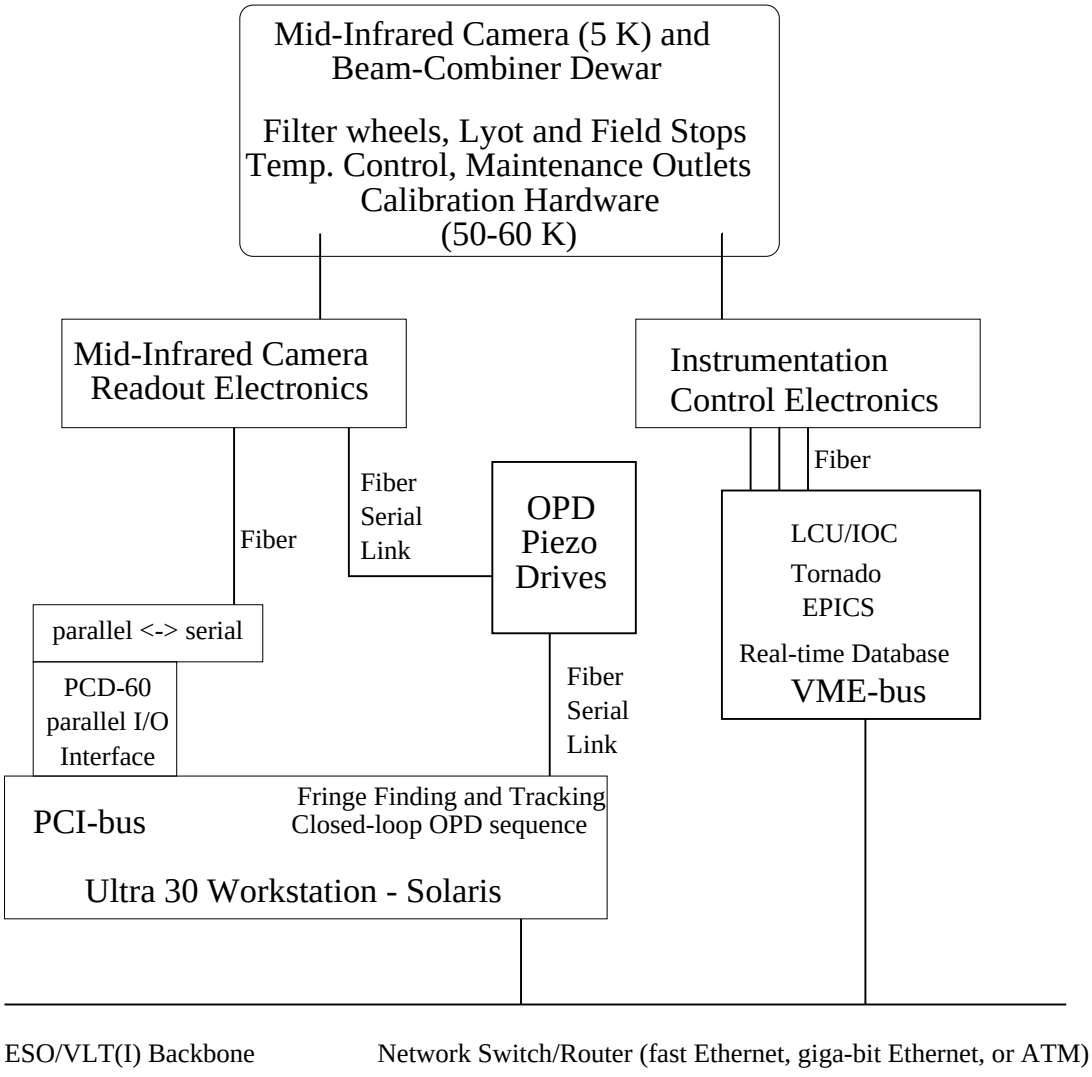

Figure 7.1: MIDI Control System Architecture

Chapter 8

Design of the Cryo-Mechanics

A major concern of the design is the thermal isolation of the low-temperature parts from room temperature and the mechanical isolation of the instrument from vibrations introduced by the closed cycle cooler.
We propose to use a two-stage Gifford-McMahon cooler from LEYBOLD (*Coolpower 4.2 GM*) with 0.5 W at 4.2 K and 50 W at 50 K. This cooler has the advantage that it runs very quiet at 144 RPM since a DC Microstepper motor driven displacer is used. To avoid resonance problems it is possible to vary the speed of the cold head motor.
Because the instrument is very sensitive at the whole thermal wavelength region all optics and mechanics inside the dewar have to be cooled to temperatures below 70 K.
The main contribution to the heat load is the radiation shield.
This heat load can be calculated in principle by (Infrared Handbook):

$$I_{2\to 1} = A_1 \sigma c (T_2^4 - T_1^4)$$

with

$$c = (\frac{1}{\epsilon_1} + \frac{A_1}{A_2}(\frac{1}{\epsilon_2} - 1))^{-1}$$

σ = Stefan-Bolzmann constant

A result can be given if the mechanical dimensions of the dewar are known. Other contributions to the heat load are the heat conduction due to the cabling, the spacers, the motor axes feed throughs and the filling tubes.
We are thinking about the alternative to use cold stepper motors inside the dewar instead of encoder equipped servo motors with feedthroughs.

The CONICA dewar is now in the test phase and therefore we will profit a lot from these experiences.

In Figure 8.1 the principal cryo-design of the MIDI-experiment is given. Figure 8.2 shows an example of how the cooling down procedure could be performed.

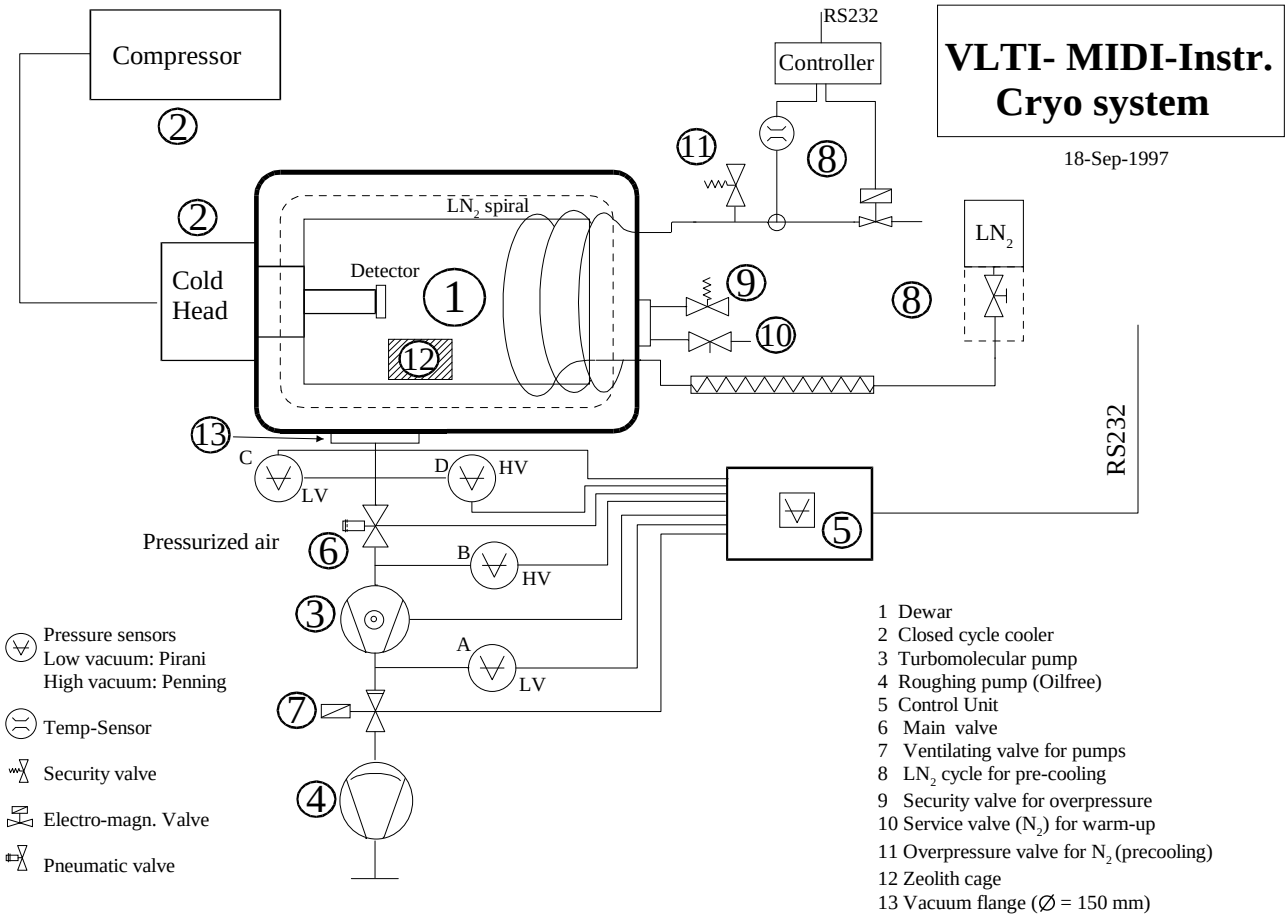

Figure 8.1: Cryo-system design for the MIDI instrument

Cooling down Procedure

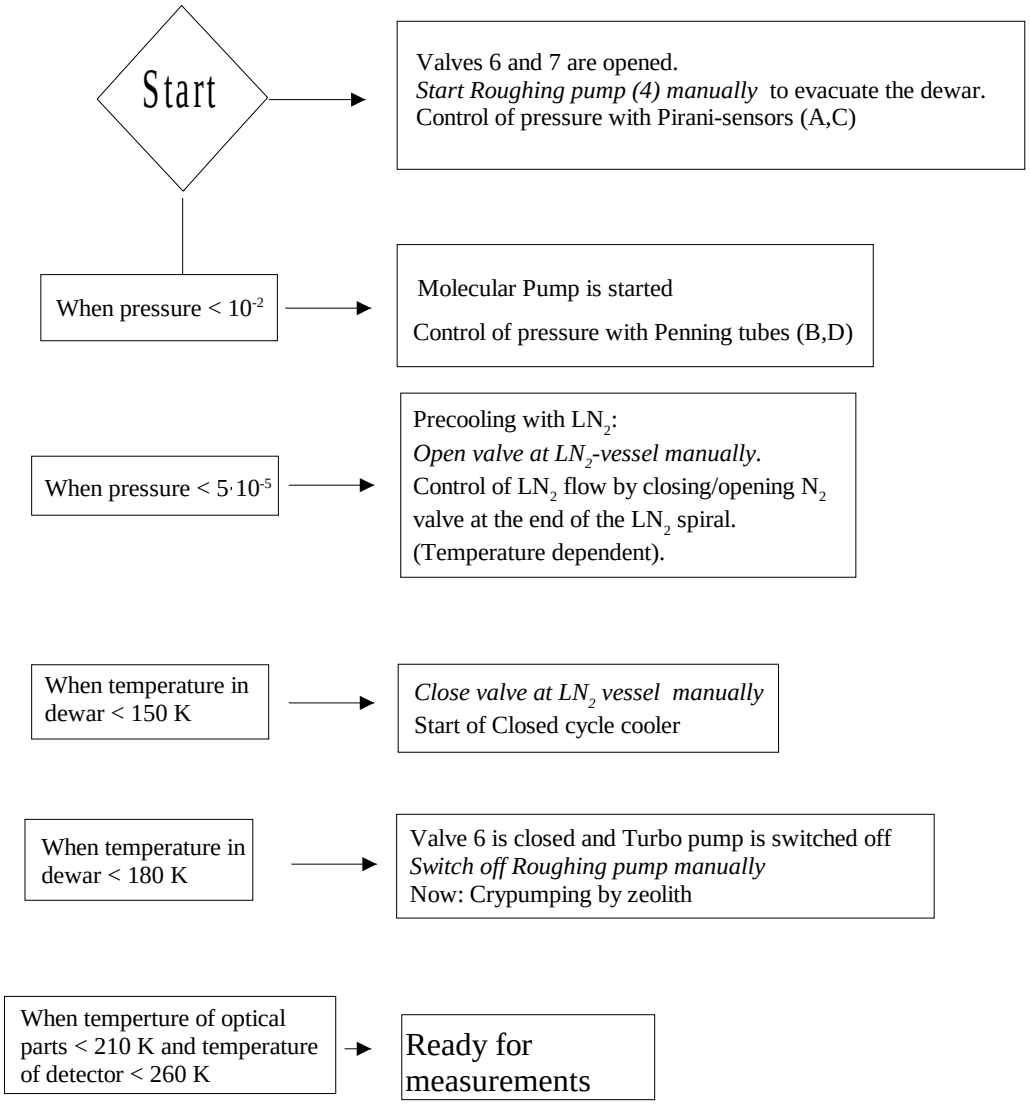

Note: Only the Roughing pump and the valve at the LN_2 vessel is operated manually

Figure 8.2: Cooling-down process for the MIDI instrument

Chapter 9

Data analysis

Taking into account the characteristics of MIDI (beam cleaning for bright sources allowed by spatial filtering and a photometric calibration), different schemes of analysis are possible depending on the brightness of the source and on the mode of acquisition. Three modes can be identified and have been experienced on other kinds of instruments:

1. coherent co-adding;
2. incoherent co-adding of spectral densities;
3. individual analysis of frames.

Table 9.1 gives the different circumstances under which these modes can be applied. In the cophased mode, the zero OPD (optical path difference) is identified with a precision of a fraction of the wavelength. In the coherenced mode, the zero OPD is known to within a few wavelengths and fringes are detected in each frame. In the blind mode, fringes are not clearly detected but are contained in each frame with a low Signal-to-Noise ratio (S/N).

Table 9.1: Data analysis modes.

	cophased mode	coherenced mode	blind mode
coherent co-adding	×		
individual frame analysis	×	×	
incoherent co-adding		×	×

In the following, it is assumed that the background has been removed from the data.

9.1 Coherent co-adding of fringe frames

This is the easiest case. The OPD or the position of the white fringe is identified or stabilized and it is possible to add all interferograms coherently in phase. Data are piled up and the signal

is integrated to improve the S/N. This mode concerns bright sources with fringes obtained with a good contrast.
This data analysis scheme can be applied whether the beams have been spatially filtered or not. Of ocurse, to obtain visibilities, a photometric calibration is needed. The accuracy of the contrast estimate depends on whether the beam cleaning has been done or not although it is not the only parameter to take into account. The S/N on the central fringe should lead to an estimate of the final contrast accuracy.

9.2 Individual analysis of frames

Phase information is not known accurately therefore it is not possible to add interferograms coherently. Nevertheless, it is still possible to recover high precision fringe contrasts. Fringe contrasts are computed frame-by-frame. The final contrast is determined from the whole contrasts distribution. The uncertainty is given by the standard deviation of the distribution.
In this mode, data are acquired with or without spatial filtering and with or without photometric calibration.
This data analysis mode can also be used when the array is cophased. It is an alternative to the previous analysis mode. This mode of analysis is currently successfully used in the FLUOR/IOTA experiment and precisions as good as 0.3% on visibility estimates have been achieved.

9.3 Incoherent co-adding of spectral densities

When the two previous data analysis processes cannot be worked out because the signal is too weak to be measured within one coherence time, a fringe signal can be recovered in the frequency domain by averaging power spectra of short exposures. The fringe contrast is computed by integrating the averaged power spectral density.
This data analysis mode should allow to observe very faint sources or sources with a very low visibility. The method can be compared to what is done in speckle interferometry analysis. Because of the weakness of the fringe signal, the beam cleaning will probably be avoided in this mode of observation. As a result, multiplicative calibration noise, additive detector and background noises will be large and the final error on visibilities is expected not to be better than 10%.

Chapter 10

Interface to ESO

- Siderostat test: collecting surfaces larger than the actually planned are necessary to test the 10 μm experiment.
Testing of the MIDI instrument on Paranal before starting to do measurements is essential. However the actual design of the VLTI siderostat test (beam size maximum: 80 to 125 mm) does not guarantee for accurate test measurements with MIDI. The following table shows the magnitude limit where we expect to see measurable fringes (S/N = 10) for different mirror sizes. As a result we note that since the sources are distributed over the whole sky and within the reach of the siderostats (an estimated $\pm 30^\circ$) only for four to six hours per night, the coverage by sources of -4 mag (provided with a mirror size of 20 cm) is only marginally sufficient for a test campaign (see Table 10.1). Only 11 sources remain over the portion of the sky accessible to the siderostats (δ = -10° to -70°), and of these only one, α Sco, can be considered a source giving a good signal, three other sources probably also are useful, and three additional ones may work marginally. We therefore urge ESO to provide siderostats of at least 20 cm in diameter, but to make serious attempts to suplly them with larger aperture.

- Chopping and nodding
Absolute calibration is needed here to calibrate the fringe amplitudes into visibilities. We propose to use standard calibration procedures for the thermal IR, i.e. chopping and nodding, interspersed with fringe measurements.

Allowing 100 ms for fringe analysis, the maximum chopping frequency turns out to be about

Table 10.1: Predicted number of sources on sky for testing of 10 μm instrument

Siderostat size	optimistic	assumptions	more realistic	assumptions
12.5 cm	-4.0 mag	11 sources	-5.0 mag	4 sources
20.0 cm	-3.0 mag	34 sources	-4.0 mag	11 sources
25.0 cm	-2.5 mag	59 sources	-3.5 mag	18 sources
32.0 cm	-2.0 mag	77 sources	-3.0 mag	34 sources

5 Hz. Nodding is required with much lower frequency. The chopping amplitude depends on the nature of the source, e.g. on whether the target is overimposed to some extended emission. The stroke value provided by ESO (15 arcsec) should be enough for most applications. Concerning the chopping accuracy, a value 27 mas rms could introduce a variation in the OPD of the same order as the OPD range we want to sample. However this should not be of concern because of the compensation provided by the tip-tilt system.
The main requirements on telescope control would be that

- chopping of telescopes is performed strictly simultaneously for all telescopes involved
- the command for chopping can be given on quite short notice (ms) when the telescope is in the appropriate mode
- the VLTI instrument is notified immediately whenever a pointing change occurs (for synchronisation purposes).

- *Actual input beams into the MIDI instrument for different kind of sources*
Estimations for the wavefront error due to all optics down to the laboratory (taking into account design, figuring, alignment, and internal seeing) and for the OPD variation have already been provided by ESO. However, for the actual operation of MIDI it is necessary to know how well the optics alignment can be kept. An initial alignment procedure and routine alignment checks will be required.

Additional topics to be investigated with ESO are: differential diffraction effects and quality of image stabilization off-axis. As far as differential diffraction is concerned, it is necessary to define a way to cross-reference the visible tip-tilt reference with that seen by the instrument at 10 μm to check whether the images at 10μm are superimposed or not, as well as to compensate for a number of misalignments.

Further, the question should be discussed where best to perform the beam compression required by most instruments: in the individual experiments or rather on system level near the entrance to the interferometric laboratory.

- *Shift of the pupil*
According to our actual study it looks preferable for MIDI to have the output pupil from the delay line shifted by about 28 m in order to bring the pupil into the cold part of the instrument. The design of the delay line comprises a variable curvature mirror to generate transfered pupil inside the interferometric laboratory. The pupil transfer range is between 10 and 80 m to keep the exit pupil stable while varying the delay line position. We would like to investigate with ESO the feasibility, within the actual design, of shifting the position of the pupil by means of the variable curvature mirror or some other measure. For similar reasons, other instruments may also be interested in some shift of the pupil.

Chapter 11

Tests

11.1 Tests with the mid-infrared camera MAX on UKIRT

In the period 17-23 October 1997 we have realized an interferometric experiment with the mid-infrared camera MAX on UKIRT. The MAX camera has a rotating wheel which allows to chose between different Lyot stops at the instrumeny-internal pupil position. The experiment consisted in inserting three pupil masks of different size, obtaining in practice two separated apertures on the UKIRT primary. The parameters of the three masks were (see Fig. 11.1):

- Two round holes with diameter 1.52 mm each, separated (center to center) by 6.4 mm. On the UKIRT primary, this corresponds to two 67 cm aperures about 2.8 m apart. Scaled to the VLTI size, this would correspond to two UTs, 35 m apart.
- Two 0.75 mm holes, separation 3.2 mm. On the UKIRT primary this corresponds to two 33 cm apertures 1.4m apart. The "VLTI equivalent" is the same as in the previous case.
- Two different holes (0.75 mm and 0.2 mm) 3.2mm apart. On the UKIRT primary, this corresponds to 33cm + 8.8cm, 1.4m apart. On VLTI, this would roughly correspond to a UT+AT system with 35 m separation.

Several sources have been observed with different filters and integration times. Fringes have been easily observed in almost every configuration. This is not surprising, since after the recent upgrades of the UKIRT telescope we routinely reach with MAX the diffraction limit at 10μm ($\lambda/D \approx 0.6''$).

Here we present a few preliminary results relative to α Ori, a [N]=-5.1 red supergiant star known to be surrounded by an ($\approx 2''$) extended dust envelope.

In Fig. 11.2 we present the image obtained by averaging 100 chopped pairs of frames (source-sky). The first (67 cm/67 cm/280 cm) mask was used, with a 11.6μm(2.5 μm) filter and an integration time of 25 ms/frame. In fig. 11.2 we also show the cut over a central column. The fringe contrast turns out to be 0.25, a factor of two less than expected from previous measurements (Degiacomi et al. 1992). Part of this loss must be due imperfect sampling of the fringe pattern because of the narrow fringe spacing.

Immediatly after taking these data, α Ori was observed with the same filter and integration time, but with the second pupil mask (33 cm/33 cm/140 cm). The result is presented in Fig. 11.3,

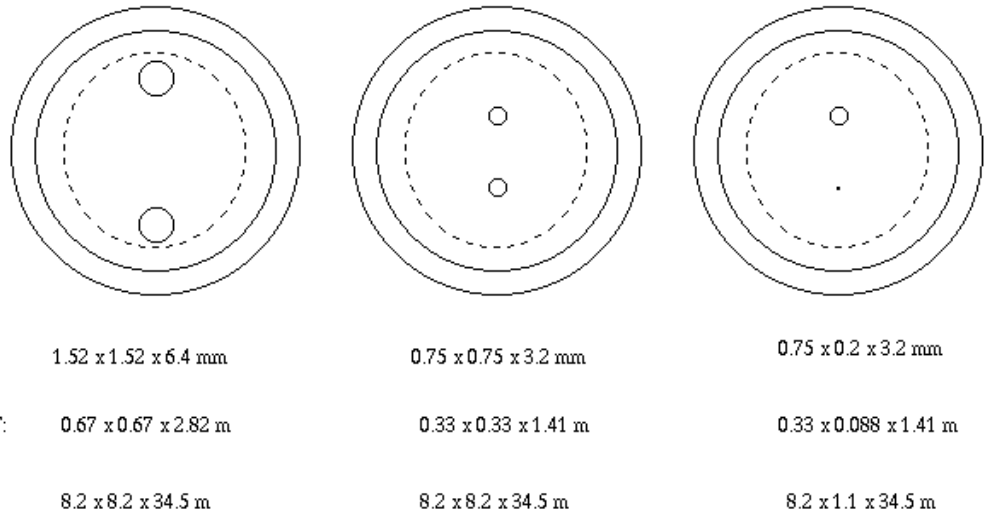

Figure 11.1: Pupil masks used in the interferometric experiment on UKIRT. For details see the text.

including the cut along a central column. The fringe contrast is in this case 0.50, the value expected if the envelope of α Ori already is resolved out in this arrangement - an assumption which remains to be checked.

These measurements require further analysis before allowing to confirm the estimated interferometric sensitivity of the MIDI instrument of N= 5 mag. This evaluation which in particular has to understand the different visibility values derived with the different masks is in progress at the present time. The telescope should not be the reason for substantial losses of visibility in the measurements. We can expect that on a baseline of 2-3 m at Mauna Kea the tip tilt correction allows to (almost) preserve the natural fringe contrast of the source.

Even when only concerning the photometric sensitivity, an estimate of the MIDI performances obtained by scaling the results of this experiment requires some caution. Our data are clearly read-out noise limited, since the cold masking of the pupil dramatically reduces the number of background photons falling on the detector (by a factor ≈ 30 with the 67 cm apertures). A sensitivity limit derived from a readout-noise limited measurement tends to be pessimistic. On the other hand, MAX on UKIRT operates under close-to-optimal conditions from the point of view of the thermal emissivity, transmission and diffraction losses; all these degrading factors are in comparison much more significant in the VLTI beam. Therefore a sensitivity estimate derived from these UKIRT measurements also will be optimistic. Anyway, if we assume for the moment that these two effects essentially cancel, we can get an order of magnitude estimate for the MIDI sensitivity to incoherent light. With our experiment with the 67 cm masks, we obtain a S/N = 47 in 25 ms (on source) for α Ori. In the readout noise limited case, this S/N scales according to the formula:

$$S/N = 4.4 \times 10^3 \frac{A_{tel}}{\sqrt{N_{pix}}}$$

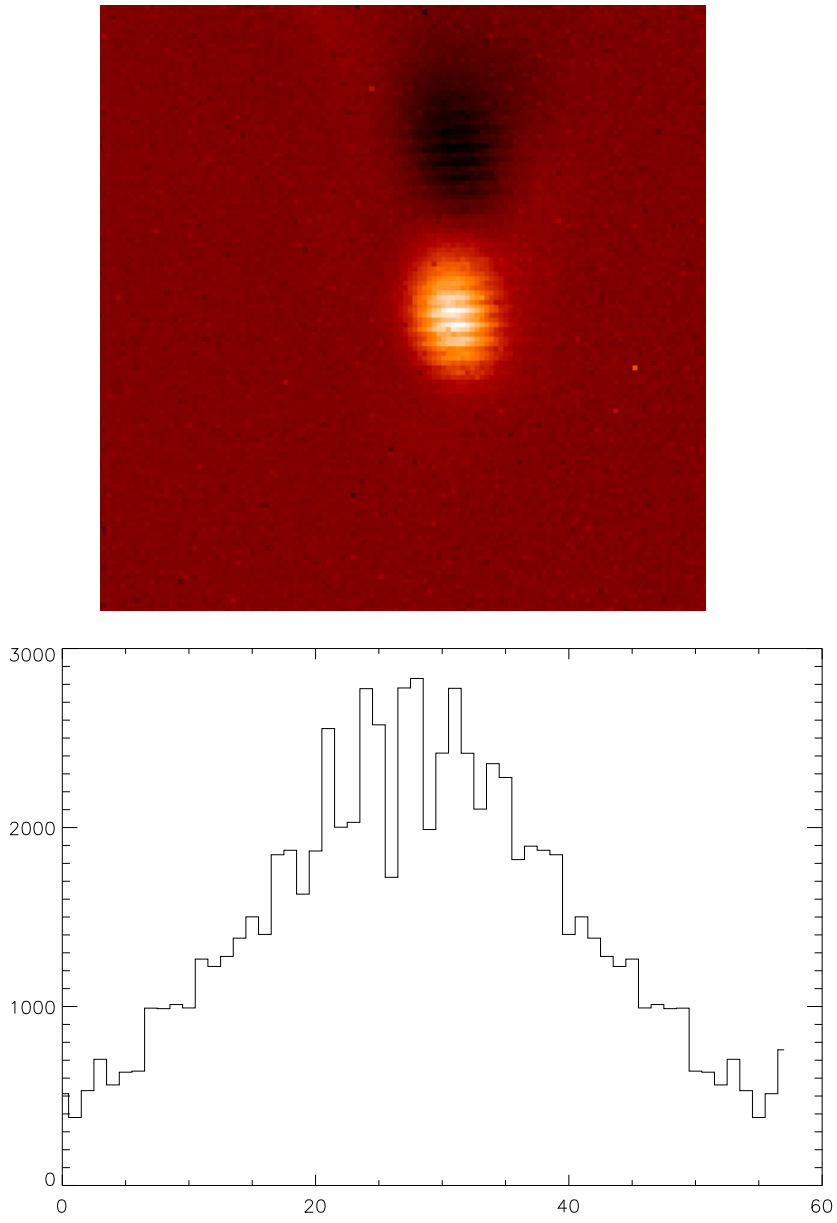

Figure 11.2: Results of the interferometric test measurement with a mask corresponding to two 67 cm apertures separated by 2.8 m. Upper part: average over 100 chopped images of 25 ms per individual exposure. Lower part: cut along a central column.

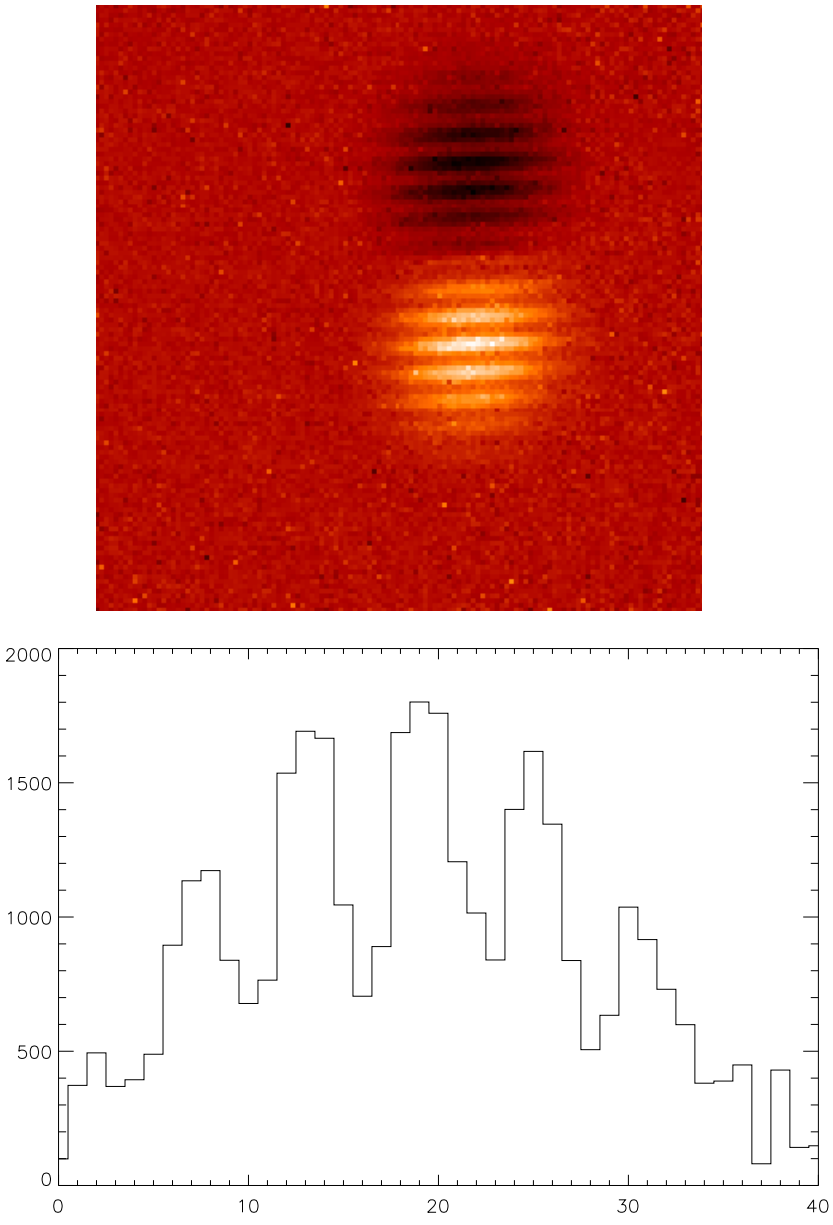

Figure 11.3: Results of the interferometric test measurement with a mask corresponding to two 33 cm apertures separated by 1.4 m. Upper part: average over 100 chopped images of 25 ms per individual exposure. Lower part: cut along a central column.

where A_{tel} is the area of the telescope in square meters. For the VLT (A_{tel} = 52 m^2, N_{pix} = 1) we get therefore a S/N =10 for a [N]=+5.8 mag source for the corresponding readout noise limited case. This value, as said above, is a preliminary deduction from the test measurements.

C.G. Degiacomi, M. Bester, W.C. Danchi, L.J. Greenhill and C.H. Townes, in "High-resolution imaging by interferometry II", eds. J.M. Beckers and F. Merkle, ESO conference and workshop proceedings No. 39, Garching 1992.

11.2 First Laboratory set-up

We have planned to install a CO_2-Laser in a Mach-Zehnder-Interferometer configuration to study fringes at a wavelength of 10μm.
The optical setup is shown in the figure 11.4. The continuous wave laser (Invar-stabilized Ultra Lasertech Model 3622) with 3.5 Watt output power works as the coherent light source. The laser is water cooled (stability=$\pm 0.01^oC$). The exact cooling and the Invar rods prevents the hopping between different laser lines. The laser has a pilot visible laser diode for safety and alignment reasons. A 10x laser beam expander will be used to expand the 3.5mm diameter laser beam. Because the 3.5 Watt output of the laser ist still to much for our experiment we will install two beamsplitters with 94% reflection in front of the 50/50 beamsplitter which splits the beam into two components. Two mirrors reflect the beams on the beam combiner. One mirror will be mounted on a translation stage for optical path modulation. As detector we will use in the initially a chopped Golay cell, later a two-dimensional array camera..
The whole experimental setup will be installed on a 3000 x 1200mm optical table. The table has an internal damping mechanism and stands on four vibration isolators.
The described experiment will be the "playground" for the first steps in interferometry at 10μm. Later this setup will also be used to test the infrared optics, to perform vibration tests (closed cycle coolers) and as a calibration source for the instrument.
The laser itself and most of the optics for the first setup will be available at the end of this year. So the first experiments will start at the beginning of 1998.

11.3 Preliminary commissioning with siderostats

We consider it essential to have the instrument running on Paranal with the VLTI delay line and light from stars before we start the commissioning on the UTs. Everything else has to be considered a waste of precious telescope time. We have already mentioned above in section 10 that at 10 μm a siderostat size of at least 20 cm is needed. Only 11 sources remain over the portion of the sky accessible to the siderostats (δ = -10° to -70°), and of these only one, α Sco, can be considered a source giving a good signal, three other sources probably also are useful, and three additional ones may work marginally. Clearly, there is the danger that lack of suitable 10 μm sources will render the commissioning of the instrument with the siderostats highly inefficient if the siderostat size is too small.

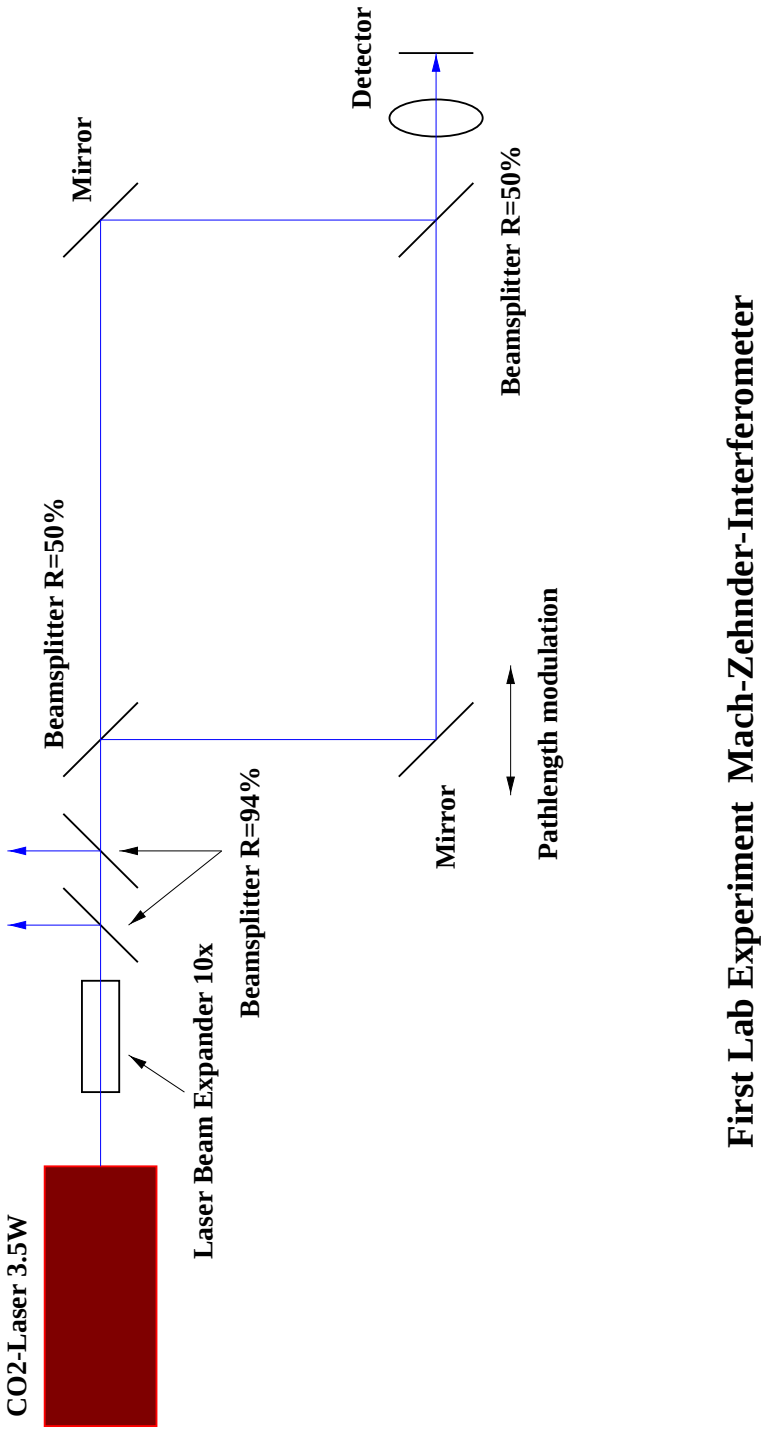

Figure 11.4: First laboratory set-up with a Mach-Zehnder interferometer

Chapter 12

Time schedule

General
The time schedule below only gives a first approach to how the project could be developing. A detailed time schedule has to be set up in connection with the accomplishment of the preliminary design.

- The decision on a larger participation in MIDI by the Netherlands will be known by the end of April 1998.
- Therefore we will not fix the design before mid-1998.
- Until the end of 1999 all parts should be ready for integration.
- Then the extensive test and calibration phase follows, starting somewhere in the first half of the year 2000 and lasting for about 6 months.
- It is planned to ship the MIDI instrument to Paranal at the end of the year 2000.
- Since the financial resources have to be spread over 3 years the time schedule for MIDI is certainly influenced by the amount of money that is available in a certain time period.
- The optical bench in the laboratory is just being built up. The first experiments with the CO_2-Laser will be done at the beginning of next year. This laboratory will be used also for the optical tests, the cryogenic tests, the integration, the final tests and the calibration.

In the following bar chart a preliminary time schedule is given for the four most important project items.

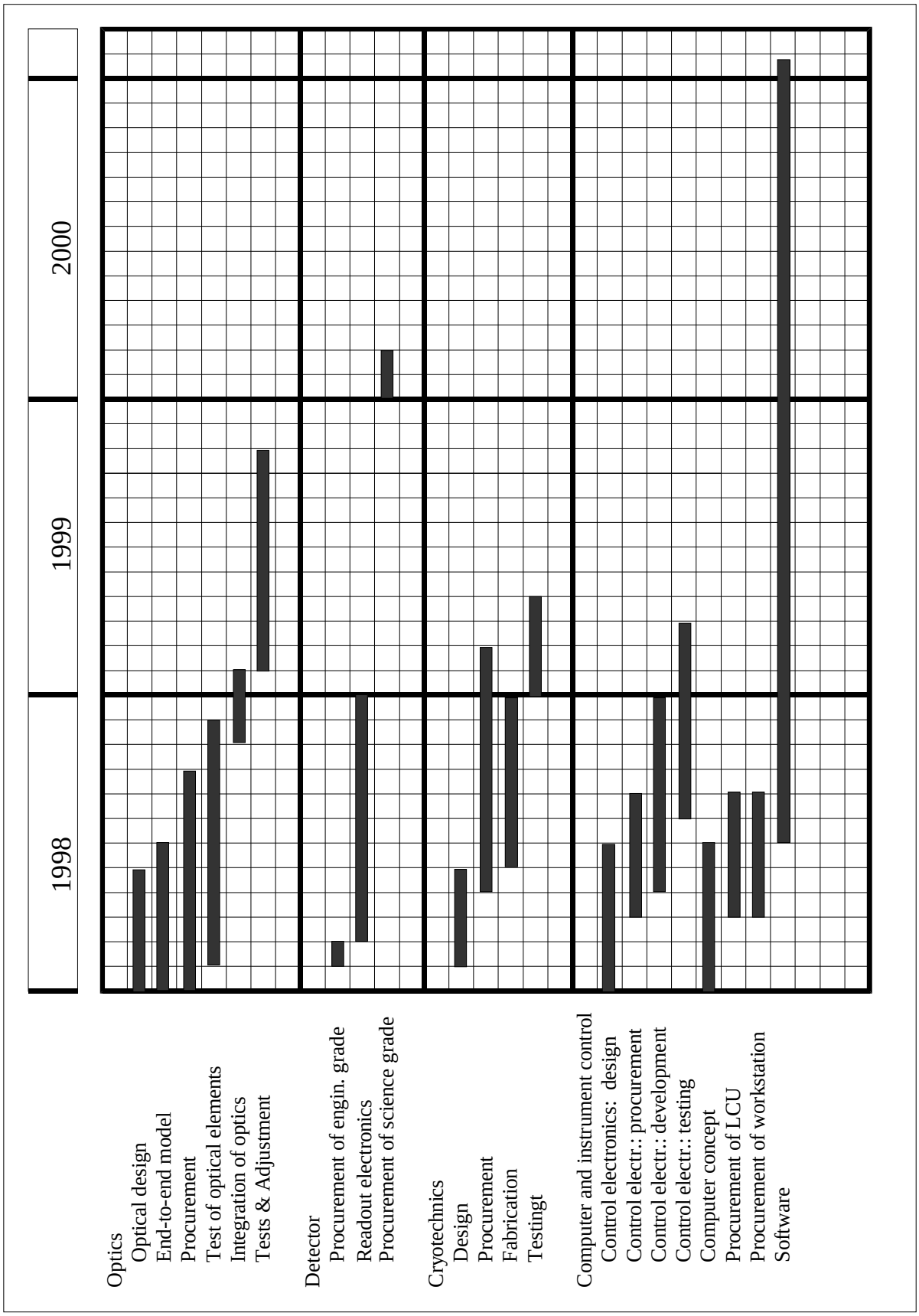

Figure 12.1: Time-schedule for the four most important items of MIDI

Chapter 13

Manpower, costs and resources

13.1 Cost Estimate for MIDI

In the following the prices are given in kDM (1000,- DM)

Total costs:

Detector	180
Detector read-out electronics	80
Data acquisition and analysis	160
Instrument control	90
Motors, encoders, housekeeping	70
Optics	230
Cryo-system	210
Mechanics	20
Laboratory, development, testing	180
Miscellaneous (not known yet)	150
Travel Costs ($\approx$10 %)	120
Total costs	1490

A breakdown of the costs for the individual subsystems is given on the following pages.

Detector:

SBRC 320 x 240 array (or Rockwell 256 x256)	170
SBRC- Engineering Grade Test-Chip	10
Total:	180

Detector read-out electronics:

Electronics (MPIA 4 ADC)	35
Additional 12 channels with 16 bit ADC (1000 fps)	45
Total:	80

Data acquisition and analysis:

Ultra 30 Sparcstation, 300 Mhz with 2 monitors, (including: 1 GB RAM, disks, backup, ATM-interface)	120
Two high speed data interfaces	10
Dual-head X-terminal	15
Network support	15
Total:	160

Instrument control:

LCU: VME-bus system serving as interface to ESO and as LCU (Transition board, MYME 177 CPU, interface, Tornado- and EPICS-software)	60
Electronics (MPIA)	20
Cables, connectors, fiber links, spare parts	10
Total:	90

Motors, encoders, housekeeping :

Two piezo-stages (100 mm) + driver for OPD-modulation	20
Piezo-Controller with DSP	2
Six encoder/motor (cryocapable) + gearing (a 2100,- DM)	13
Six encoder/motor + gearing (outside dewar)	4
Twelve motion controller	6
Temperature Measurement controller	4
Temperature sensors (Si-diodes and Pt 100)	1
Detector temperature controller	5
Five Process-controller (for warm-up heaters, ..)	3
Interlock modules for safe cool-down and warm-up procedure	2
Divers	10
Total:	70

Optics:

Plane mirrors:	Outside dewar (OPD (8), feed-in (5), ...)	15
	Inside dewar (8)	10
Reflective Optics:	2 Beam-reducer (Cassegrain)	20
	4 Off-axis paraboloids	20
	2 Toroidals	10
Beamcombiner		20
2 Beamsplitters	(90:10, photometric beams)	5
2 Dichroics	(10/20 μm separation)	10
4 Filter (a 2500,- DM)		10
Grism or grating		30
Windows and Field stops		5
2 Camera system2 (with 2 Lenses)		10
Slits and pupil masks		3
Calibration	source/comparison light	1
Stages, holders		10
Planning costs:	Optical computation (verification)	15
Divers		36
Total:		230

Mechanics

Instrument alignment set-up	10	
Divers		10
Total:		20

Cryo-system:

Cryostat housing (MPIA)	30
Closed cycle cooler Leybold 4.2GM	65
External N2 Tank, handling tools	5
Roughing pump Leybold D40B (Prepumping to 10^{-2})	12
Turbomolecular pump + controller (10^{-2} to 10^{-5})	25
Vacuum measuring system Balzers TPG300	9
Seven Valves	10
Six feedthroughs (a 2000,- DM)	12
Shock absorbers, O-rings, etc.	5
Tubes (500,- DM per 2 m)	5
vacuum connectors	10
Maintenance carriage, divers	22
Total:	210

Laboratory, development, testing

Two local PC (labtop with desktop)	12
Numerical analysis software	12
(MathLab for VLTI end-to-end model, Optic program, etc.)	
CO_2 Laser	26
Water cooler	5
Beam adaption:	
In size (Lenses)	4
In flux (2 Beamsplitters 94:6)	5
Mirrors, Optics:	15
Pyroelectric array camera	30
2 Polarizers	9
Stages, Mechanical parts	20
Divers	42
Total:	180

Notes:

1. no spare parts included in cost estimate
2. Detector: SBRC: 96 k$, Rockwell 256 x 256: 100 k$
   If 32 read-out channels needed: 3500,- DM per channel $\rightarrow$ + 56000,- DM
3. Piezo Unit with stroke of 100 μm, including control unit and absolute positioning: 10 kDM
4. Beam-divider with 50:50, glass plate: 2 kDM, Charge for coating: 15 kDM
5. Alu-Mirror: Mirror: 6 kDM, coating: 1.5 kDM
6. Filter: typically 2 ... 4 kDM
7. Travel costs: good estimate is 10% of total costs

13.2 Needed manpower, resources

We estimate that a total of 15 manyears will be necessary to develop the mid-infrared interferometric instrument. Of these, about two manyears can be contributed by the Kiepenheuer Institut für Sonnenphysik in Freiburg by Meudon Observatory and by the Landessternwarte Thüringen.

A major uncertainty in the amount of the finally available resources is the pending application of the Dutch members of our study group, which right now has mastered the pre-selection stage, and which will be decided by May 1, 1998.

Apart from the financial contributions of the Meudon Observatory and of the Kiepenheuer Institut für Sonnenphysik, totalling about 200.000.- DM, the costs have to be covered from the budget of the Max-Plamck-Institut für Astronomie over the three year span assigned to the project.

For completeness we repeat our assumption that ESO will take over travel costs to Paranal for testing, commissioning or observing with the instrument.